29 Weis, J., Kaussen, M., Calvo, S. and Buonanno, A. (2000) Denervation induces a rapid nuclear accumulation of MRF4 in mature myofibers *Dev. Dyn.*, **218**, 438–451

30 Zhou, Z. and Bornemann, A. (2001) MRF4 protein expression in regenerating rat muscle. *J. Muscle. Res. Cel. Motil.*, **22**, 311–316

31 Campanelli, J.T., Roberds, S.L., Campbell, K.P. and Scheller, R.H. (1994) A role for dystrophin-associated glycoproteins and utrophin in agrin-induced AChR clustering. *Cell*, **77**, 663–674.

32 Kahl, J. and Campanelli, J.T. (2003) A role for the juxtamembrane domain of beta-dystroglycan in agrin-induced acetylcholine receptor clustering *J. Neurosci.*, **23**, 392–402.

33 Jacobson, C., Cote, P.D., Rossi, S.G., Rotundo, R.L. and Carbonetto, S. (2001) The dystroglycan complex is necessary for stabilization of acetylcholine receptor clusters at neuromuscular junctions and formation of the synaptic basement membrane *J. Cell Biol.*, **152**, 435–450

34 Saito, F., Moore, S.A., Barresi, R., Henry, M.D., Messing, A., Ross-Barta, S.E., Cohn, R.D., Williamson, R.A., Sluka, K.A., Sherman, D.L., *et al.* (2003) Unique role of dystroglycan in peripheral nerve myelination, nodal structure, and sodium channel stabilization *Neuron*, **38**, 747–758.

35 Leschziner, A., Moukhles, H., Lindenbaum, M., Gee, S.H., Butterworth, J., Campbell, K.P. and Carbonetto, S. (2000) Neural regulation of alpha-dystroglycan biosynthesis and glycosylation in skeletal muscle. *J. Neruochem.*, **74**, 70–80.

36 Ishii, H., Hayashi, Y.K., Nonaka, I. and Arahata, K. (1997) Electron microscopic examination of basal lamina in Fukuyama congenital muscular dystrophy. *Neuromuscul. Disord.*, **7**, 191–197.

37 Nagel, A., Lehmann-Horn, F. and Engel, A.G. (1990) Neuromuscular transmission in the mdx mouse. *Muscle Nerve*, **13**, 742–749.

doi:10.1093/brain/awl077 Brain (2006), 129, 1470–1480

Central core disease is due to *RYR1* mutations in more than 90% of patients

Shiwen Wu,[1] Carlos A. Ibarra M,[1] May Christine V. Malicdan,[1] Kumiko Murayama,[1] Yasuko Ichihara,[2] Hirosato Kikuchi,[3] Ikuya Nonaka,[1] Satoru Noguchi,[1] Yukiko K. Hayashi[1] and Ichizo Nishino[1]

[1]Department of Neuromuscular Research, National Institute of Neuroscience, National Center of Neurology and Psychiatry (NCNP), Kodaira, [2]Department of Anesthesiology, Tokyo Rinkai Hospital, Tokyo and [3]Department of Anesthesiology, Saitama Medical School, Saitama, Japan

Correspondence to: Ichizo Nishino, MD, PhD, Department of Neuromuscular Research, National Institute of Neuroscience, National Center of Neurology and Psychiatry (NCNP), 4-1-1 Ogawahigashi-cho, Kodaira, Tokyo 187-8502, Japan
E-mail: nishino@ncnp.go.jp

Ryanodine receptor 1 (*RYR1*) gene mutations are associated with central core disease (CCD), multiminicore disease (MmD) and malignant hyperthermia (MH), and have been reported to be responsible for 47–67% of patients with CCD and rare cases with MmD. However, to date, the true frequency and distribution of the mutations along the *RYR1* gene have not been determined yet, since mutation screening has been limited to three 'hot spots', with particular attention to the C-terminal region. In this study, 27 unrelated Japanese CCD patients were included. Clinical histories and muscle biopsies were carefully reviewed. We sequenced all the 106 exons encoding RYR1 with their flanking exon–intron boundaries, and identified 20 novel and 3 previously reported heterozygous missense mutations in 25 of the 27 CCD patients (93%), which is a much higher mutation detection rate than that perceived previously. Among them, six were located outside the known 'hot spots'. Sixteen of 27 (59%) CCD patients had mutations in the C-terminal 'hot spot'. Three CCD patients had a probable autosomal recessive disease with two heterozygous mutations. Patients with C-terminal mutations had earlier onset and rather consistent muscle pathology characterized by the presence of distinct cores in almost all type 1 fibres, interstitial fibrosis and type 2 fibre deficiency. In contrast, patients with mutations outside the C-terminal region had milder clinical phenotype and harbour more atypical cores in their muscle fibres. We also sequenced two genes encoding RYR1-associated proteins as candidate causative genes for CCD: the 12 kD FK506-binding protein (*FKBP12*) and the α1 subunit of L-type voltage-dependent calcium channel or dihydropyridine receptor (*CACNA1S*). However, no mutation was found, suggesting that these genes may not, or only rarely, be responsible for CCD. Our results indicate that CCD may be caused by *RYR1* mutations in the majority of patients.

Keywords: central core disease; genotype–phenotype correlation; muscular dystrophy; myopathy; ryanodine receptor 1 mutations

Abbreviations: CACNA1S = α1 subunit of L-type voltage-dependent calcium channel; CCD = central core disease; CICR = calcium-induced calcium release; EC = excitation–contraction; *FKBP12* = FK506-binding protein, 12 kD; mGT = modified Gomori–Trichrome; MmD = multiminicore disease; MH = malignant hyperthermia; *RYR1* = ryanodine receptor 1; SERCA = sarco-endoplasmic reticulum Ca^{2+} ATPase; SR = sarcoplasmic reticulum

Received October 28, 2005. Revised March 1, 2006. Accepted March 8, 2006. Advance Access publication April 18, 2006

Introduction

Central core disease (CCD) was the first described congenital myopathy in humans (Shy and Magee, 1956), usually inherited in an autosomal dominant pattern, except for few reports on autosomal recessive cases (Manzur *et al.*, 1998; Jungbluth *et al.*, 2002). The clinical features are quite variable (Quinlivan *et al.*, 2003), ranging from lack of visible weakness or abnormality to lack of independent ambulation. Most of the patients, in classical descriptions, have a slowly or

non-progressive proximal muscle weakness and hypotonia during infancy that can persist throughout adolescence/adulthood, and have associated delayed motor development and reduced muscle bulk. In addition, musculoskeletal alterations including congenital hip dislocation, kyphoscoliosis and joint contractures are also common findings in CCD patients (Lorenzon *et al.*, 2000; Quinlivan *et al.*, 2003). The diagnosis is commonly made from muscle biopsy by the presence of cores in type 1 fibres, which are typically well demarcated and located centrally in the fibres. A few cores, however, can be located in the subsarcolemmal regions of individual type 1 muscle fibres. Longitudinal sections show that the core runs the whole length of the fibre.

Recent reports have documented that the phenotypic presentation varies considerably from no visible disability to lack of independent ambulation. While the overall incidence of CCD is rare, the absence of symptoms in a significant number of patients may suggest that the actual incidence of CCD may be considerably higher than that perceived currently.

CCD has been linked to the gene encoding the skeletal muscle ryanodine receptor, *RYR1*, and is considered to be an allelic disease of malignant hyperthermia (MH) susceptibility. This is a pharmacogenetic disorder with autosomal dominant inheritance in which susceptible individuals develop generalized muscle contracture followed by a hypermetabolic state due to massive calcium release from the sarcoplasmic reticulum (SR), when they are exposed to inhaled general anaesthetics or to the depolarizing muscle relaxant succinylcholine. CCD patients have higher probability to be susceptible to MH. The *RYR1* mutations linked to MH and CCD are clustered in three relatively restricted regions of the protein or 'hot spots': N-terminal (residues p.M1-R614), central (p.R2163–p.R2458) and C-terminal (p.R4136-p.P4973). They are also called domains 1–3, respectively (Treves *et al.*, 2005). The first two domains are located in the soluble cytoplasmic regions of the protein. Most of the CCD mutations are clustered in domain 3, which is located in the C-terminus and comprises the transmembrane/luminal and pore-forming region of the channel (McCarthy *et al.*, 2000; Monnier *et al.*, 2001; Davis *et al.*, 2003). Hence, mutations in this region of the protein may directly alter the permeation/selectivity/gating properties of the channel (Balshaw *et al.*, 1999).

The *RYR1* is one of the largest described genes in humans, spanning >159 kb in size on chromosome 19.q13.1. A 15 117-nucleotide-long open reading frame encoded in 106 exons (two of which are alternatively spliced) produces a 563 kD protein. In addition, it forms a homotetrameric structure that functions as an SR calcium-release channel regulating Ca^{2+} content in skeletal muscle during excitation–contraction (EC) coupling. Because of the size of the *RYR1* gene, efficient routine screening for mutations has been difficult. Most of the *RYR1* mutation screenings in CCD patients have been limited to the above-mentioned three 'hot spots' or even to the C-terminal region alone, and 47–67% patients were found carrying *RYR1* mutations (Monnier *et al.*, 2001; Davis *et al.*, 2003; Shepherd *et al.*, 2004), which suggested that CCD is a genetically heterogeneous disease. Here, we screened all the exons and flanking exon–intron boundaries of *RYR1* in order to determine the frequency and distribution of mutations, and describe the genotype–phenotype correlation in Japanese patients with CCD.

Although no mutation in other genes has been associated with CCD, many studies have shown that mutants of the RYR1-associated proteins FKBP12 and CACNA1S cause EC uncoupling *in vitro* just as some *RYR1* mutants do (Avila *et al.*, 2003*b*; Lyfenko *et al.*, 2004; Weiss *et al.*, 2004), raising a possibility that *FKBP12* and/or *CACNA1S* mutations may also be responsible for CCD. In addition, the mutations in the *RYR1*-binding domain of *CACNA1S* are thought to account for 1% of MH patients (Stewart *et al.*, 2001). We therefore sequenced the entire open reading frame of *FKBP12* and the part of *CACNA1S* that encodes the *RYR1*-binding region.

Methods

Subjects

Unrelated Japanese CCD patients were selected for the study from the *National Center of Neurology and Psychiatry (NCNP)* database from 1982 to 2004. CCD diagnosis was established on the basis of characteristic muscle pathology findings of cores almost exclusively in type 1 fibres. We excluded multiminicore disease (MmD) cases, which had multiple cores in >70% of type 1 fibres in our series. Available blood samples from the patients' relatives were also included in the analysis. In addition, DNA samples from 150 subjects without any known muscle disease were studied. Informed consent was obtained from the patients or their parents, as well as from control subjects.

The patients' clinical features were assessed by careful review of their medical records. Pathological features of all patients were independently evaluated by four authors (S.W., M.C.V.M., I.N. and I.N.). All patients have undergone a battery of histochemical stains, including haematoxylin and eosin, modified Gomori–trichrome (mGT), NADH-tetrazolium reductase (NADH-TR) and myosin ATPase.

In order to evaluate the genotype–phenotype correlation in CCD patients, the patients were divided into four groups, respectively, provided that they had one heterozygous C-terminal mutation, one heterozygous non-C-terminal mutation, two heterozygous mutations or no mutation.

Data were entered in Statistics Software for Social Sciences (SPSS version 11.0). Demographic characteristics were analysed by computation of the frequency, the mean ± standard deviation (SD), or the mean ± standard error of means (SEM), whichever was appropriate. The data then were subjected to a univariate analysis (Fisher's exact test). For comparing age and type 2 fibre deficiency, Mann–Whitney test was employed.

Mutational analysis

Genomic DNA was extracted from either muscle biopsy samples or peripheral blood lymphocytes according to standard protocols (Sambrook *et al.*, 2001). PCR primers were designed to amplify all 106 exons of *RYR1*, all five exons of *FKBP12* and the seven

exons of *CACNA1S* (exon 14–17 and 25–27) that encode the RYR1-interacting region (Peng *et al.*, 1998). Amplified fragments were directly sequenced using BigDye Terminator® v3.1 Cycle Sequencing kits on ABI3100 automated Genetic Analyzer (Applied Biosystems™, USA). DNA sequences were analysed with the SeqScape program and compared with the reference genomic sequence of: *RYR1* (Genbank J05200), *FKBP12* (Genbank M92423) and *CACNA1S* (Genbank L33798).

Results

Patients

A total of 27 unrelated Japanese CCD patients were selected for the study, consisting of 7 males and 20 females (Table 1) ranging in age from 2 to 63 years [29 ± 19 years (mean ± SD)] at the time of muscle biopsy. DNA from the parents of two patients (Patients 23 and 25) were also studied.

Patients 1–8 underwent muscle biopsy because they had pertinent family history of MH and were considered to be MH susceptible. In Japan, the diagnosis of MH susceptibility is achieved by detecting enhancement in the rate of calcium-induced calcium release (CICR) from the sarcoplasmic reticulum in chemically skinned muscle fibres (Ibarra *et al.*, 2005), reflecting the underlying pathomechanism of this disorder, that is, a lower activation threshold of the SR calcium-release channel. Cores were incidentally found in the muscle biopsies of Patients 1–8; thus a working diagnosis of CCD was made despite the absence of any muscle symptoms in most of these patients. CICR rate was enhanced in all eight patients. There was no description about the MH susceptibility status on the medical records of other subjects (Patients 9–27).

Nemaline bodies were identified in Patients 11, 12 and 23 on mGT stain; hence they were labelled as having core/rod disease (CRD).

Mutations

A total of 23 different missense mutations affecting 19 residues in *RYR1* were identified, consisting of 3 previously reported and 20 newly identified missense mutations in 93% of CCD patients (Tables 1 and 2). Two patients did not have any mutation in *RYR1*. All mutations were heterozygous single nucleotide changes, except for the substitution of two consecutive nucleotides (c.14761_14762TT>AC) in Patient 21, which was predicted to result in a single amino acid change (p.F4921T). There were two common heterozygous *RYR1* mutations in this cohort: c.14581C>T (p.R4861C) and c.7522C>G (p.R2508C), identified in 4 out of 25 (16%) and in 3 out of 25 (12%) patients, respectively. No mutations were found in either *FKBP12* or *CACNA1S*.

Twenty-two of 25 (88%) had only one heterozygous mutation: 14 (56%) with a heterozygous C-terminal mutation and 8 (32%) with a heterozygous non-C-terminal mutation. The remaining three (12%) patients had two heterozygous mutations (Patients 23, 24 and 25). Only the parents of Patients 23 and 25 were screened for the respective pair of mutations, as samples were not available from the parents of Patient 24. In Patient 23, the mutation p.D60N was identified in exon 3 of her maternal allele while p.L3606P was found in exon 73 of her paternal allele. In Patient 25, p.E512K in exon 14 was inherited from her mother while p.R4893P in exon 102 was acquired from her father. No muscle samples were available for histological studies from the parents of these two patients. *RYR1* mutations were found in patients with CRD (Patients 11, 12 and 23) (Table 1, Fig. 1). None of the newly identified missense mutations were found in 300 control chromosomes. Eighteen of 19 amino acids predicted to be changed were highly conserved through *RYR1* evolution and most of them were also conserved across the *RYR* species, *RYR1*, *RYR2* and *RYR3* (Table 2).

The mutations found in this cohort of CCD patients are shown in Fig. 2 at their respective location in the *RYR1*, along with those reported previously. In this study, 6 mutations were located outside the mutational 'hot spots', 4 in N-terminal 'hot spot' and 13 in the C-terminal region. These mutations were carried by 8 out of 25 (32%), 4 out of 25 (16%) and 16 out of 25 (59%) patients, respectively. We did not find any mutation in the central 'hot spot' or domain 2 in our cohort.

Genotype–phenotype correlation

Among eight patients with a heterozygous non-C-terminal mutation, two showed mild limb muscle weakness while the others were asymptomatic. The exact age of onset was difficult to ascertain because of the paucity of symptoms. Significant clinical findings during pregnancy and birth were not reported in this group. On muscle histochemistry, type 2 fibre deficiency was seen in only one patient, as he had <1% of type 2 fibres, while these were >12% in others [37 ± 4% (mean ± SD)]. Minimal endomysial fibrosis was found in three patients (37%), while the others had no increase in the interstitial fibrous tissue.

In contrast, limb muscle weakness was present in all patients with C-terminal mutations, and significant symptoms were manifested during the perinatal period (Table 1). There was statistically significant association between the presence of mutation in the C-terminal domain and clinical phenotypic characteristic in the following categories: limb muscle weakness, poor foetal movement during pregnancy, presence of joint dislocation and delayed motor milestone (Fig. 3A). Endomysial fibrosis and type 2 fibre deficiency were observed in most, if not all, patients with C-terminal mutations (Fig. 3B).

In terms of core structure, most patients had single cores (95% of fibres), but multiple cores were also seen especially in patients with heterozygous non-C-terminal mutations. In mutations outside domain 3, most cores were located in the periphery or subsarcolemmal areas (71%). In patients with C-terminal mutations, cores were noted to be

Table 1 Summary of clinical and pathological features of the patients and *RYR1* mutations

Patient	Sex	Pregnancy and birth symptoms	Family history	Onset	Clinical symptoms					CICR	Type 2 fibres†	Type 1 fibres with cores†	Features of cores§					Nemaline bodies	Endomysial fibrosis	RYR1 mutations (Exon)
					Delayed motor milestone	Muscle weakness	Skeletal and/or articular malformation	Others	Age at biopsy (years)				Central cores	Rimmed' cores	Atypical cores	Single core	Multiple cores			
1	F	N	Yes	Ad	No	No	JC		25	E	32	93	15	39	20	83	17	No	Minimal	c.1422G>T, p.Q474H (13)*
2	F	N	Yes	Ad	No	D	Sc	Ptosis	37	E	27	93	22	9	12	96	4	No	No	c.7522C>T, p.R2508C (47)*
3	F	N	No	Ad	No	No			63	E	13	89	22	17	4	92	8	No	No	c.7522C>T, p.R2508C (47)*
4	F	N	No	Ad	No	No	Sc		35	E	13	84	14	11	14	84	16	No	No	c.7522C>T, p.R2508C (47)*
5	F	N	Yes	Ch	No	No	Sc		9	E	40	98	74	12	5	96	4	No	No	c.7522C>G, p.R2508G (47)*
6	M	N	Yes	Ad	No	No			34	E	65	78	14	39	10	86	14	No	No	c.7523G>A, p.R2508H (47)*
7	F	N	No	Ch	No	P			8	E	<1	39	28	9	12	89	11	No	Minimal	c.7635G>C, p.E2545D (48)*
8	M	N	Yes	Ad	No	No			48	E	75	24	43	8	27	99	1	No	Minimal	c.10100A>G, p.K3367R (67)*
9	F	N	No	Ch	Yes	P			4	ND	<1	99	34	75	1	>99	1	No	Moderate	**c.13703T>C, p.L4568P (94)***
10	F	PFM, FI, RI, PS	No	Bi	Yes	P	JD, JC		3	ND	1	99	78	62	1	100	0	No	Marked	**c.13891T>A, p.Y4631N (95)***
11	M	FI	No	In	Yes	G	JD, JC		3	ND	2	68	41	71	28	100	0	Yes	Moderate	**c.13900G>A, p.E4634K (95)***
12	F	PFM, FI	Yes	Bi	Yes	G	JD, JC		2	ND	1	98	12	88	1	100	0	Yes	Minimal	**c.13912G>A, p.G4638S (95)***
13	F	PFM	No	Ch	Yes	P	JC, Sc	FMI, HAP	3	ND	<1	86	80	70	13	98	2	No	Marked	**c.14572A>G, p.N4858D (101)***
14	F	FI	No	In	No	G	JD, JC, Sc		10	ND	1	99	81	74	15	99	1	No	Marked	**c.14581C>T, p.R4861C (101)**
15	M	N	No	Ch	Yes	P			10	ND	<1	99	86	80	1	>98	2	No	Minimal	**c.14581C>T, p.R4861C (101)**

16	F	RI, PS	No	Bi	Yes	P	JD, JC, Sc, Lo		2	ND	3	60	69	78	3	98	2	No	Marked	**c.14581C>T, p.R4861C (101)**
17	F	PFM	No	Ch	Yes	G	JD, Sc		2	ND	<1	98	58	76	5	99	1	No	Marked	**c.14581C>T, p.R4861C (101)**
18	M	N	No	Ch	Yes	P	JC, Lo		3	ND	<1	99	67	80	2	99	1	No	Minimal	**c.14582G>A, p.R4861H (101)**
19	F	PFM, FI, RI	No	Bi	Yes	G	JD, Sc	FMI	2	ND	<1	83	21	55	36	100	0	No	Minimal	**c.14693T>C, p.I4898T (102)***
20	F	PFM, FI	No	Ch	Yes	P			9	ND	<1	96	97	72	4	99	1	No	Minimal	**c.14759C>A, p.T4920N (102)***
21	M	N	Yes	Ch	No	P	Lo		6	ND	<1	>99	74	86	6	99	1	No	Minimal	**c.14761_14762TT>AC, p.F4921T (102)***
22	M	PFM, FI, RI	No	Bi	Yes	P	JD, Sc	FMI	3	ND	<1	99	34	82	23	82	18	No	Marked	c.14762T>C, p.F4921S (102)*
23	F	FI	Yes	In	Yes	P	Lo		5	ND	9	66	12	12	30	98	2	Yes	Moderate	c.178G>A, p.D60N (3); c.10817T>C, p.L3606P (73)*
24	F	FI, RI, PS	No	Bi	Yes	G	JD, Lo		10	ND	<1	14	58	62	9	99	1	No	No	c.1280C>T, p.S427L (13); **c.14696G>A, p.G4899E (102)***
25	F	FI, RI, PS	No	Bi	Yes	P	JD, Lo		2	ND	21	>99	89	66	29	98	2	No	Moderate	c.1534G>A, p.E512K (14); **c.14678G>C, p.R4893P (102)***
26	F	N	Yes	Ch	Yes	P	Sc		36	ND	13	99	94	0	74¶	98	2	No	Minimal	Not detected
27	F	N	No	Ad	No	D			35	ND	72	52	60	18	31	100	0	No	None	Not detected

C-terminal mutations are written in bold letters. F = female; M = male; N = normal; Ad = adolescence; Ch = childhood; Bi = birth; In = infancy; PFM = poor foetal movement; FI = floppy infant; RI = respiratory insufficiency; PS = poor sucking; JC = joint contracture, JD = joint dislocation; Sc = scoliosis; Lo = lordosis; FMI = facial muscle involvement; HAP = high-arched palate; D = distal, P = proximal, G = generalized; CICR = calcium-induced calcium release; E = enhanced; ND = not done. * Novel mutations; §Values expressed as percentage of cores; †Values expressed as percentage of fibres; ¶Refer to text and/or figure for description of cores.

Table 2 Comparison of amino acid in the affected residues with that from mouse, pig, rabbit and other human RYR proteins, RYR2 and RYR3

Residue	60	427	474	512	2508	2545	3367	3606	4568	4631	4634	4638	4858	4861	4893	4898	4899	4920	4921
Predicted change	N*	L*	H*	K*	G/H/C*	D*	R*	P*	P*	N*	K*	S*	D*	H/C	P*	T	E*	N*	S/T*
RyR1																			
Human	D	S	Q	E	R	E	K	L	L	Y	E	G	N	R	R	I	G	T	F
Mouse	D	S	Q	E	R	E	K	L	L	Y	E	G	N	R	R	I	G	T	F
Pig	D	S	Q	E	R	E	K	L	L	Y	E	G	N	R	R	I	G	T	F
Rabbit	D	S	Q	E	R	E	K	–	L	Y	E	G	N	R	R	I	G	T	F
RyR2																			
Human	D	K	Q	E	R	D	K	L	L	Y	E	G	N	R	R	I	G	T	F
RyR3																			
Human	D	–	Q	M	R	E	K	V	L	Y	Q	G	N	R	R	I	G	T	F

*Novel mutations.

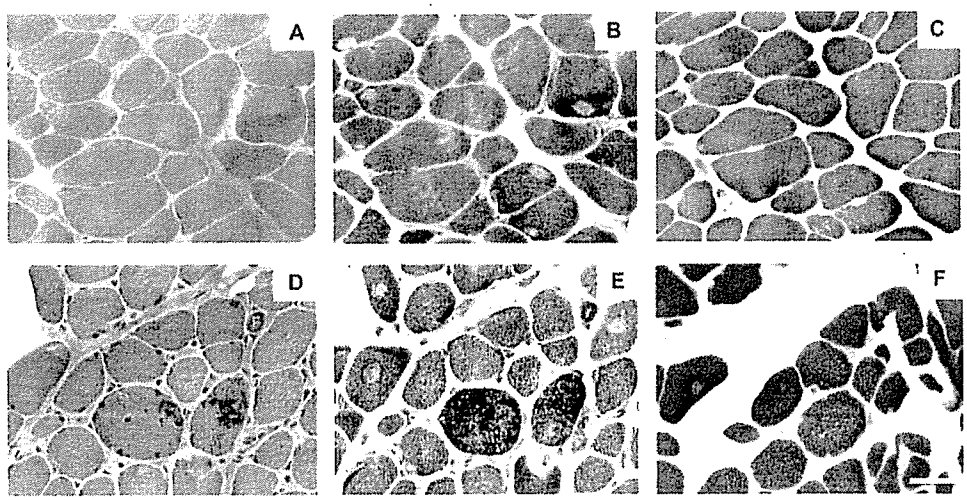

Fig. 1 Muscle biopsy. (**A–C**) A 10-year-old patient with a double mutation. (**A**) Minimal fibrosis is observed in mGT section. (**B**) NADH shows cores in type 1 fibres. (**C**) ATPase staining at pH 4.6 shows type 2 fibre deficiency. (**D–F**) A 3-year-old with nemaline bodies in muscle fibres. (**C**) Nemaline bodies and moderate fibrosis are depicted in mGT section. (**D**) Fibres with nemaline bodies have high enzymatic activity; typical central cores are noted. (**E**) ATPase staining with pH 4.3 pre-incubation demonstrates type 2 fibre deficiency. Bar denotes 50 microns.

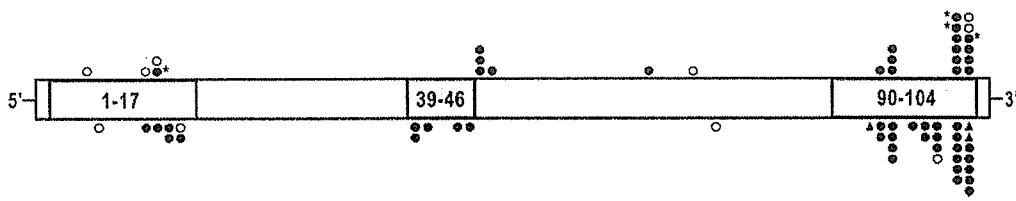

Fig. 2 *RYR1* mutation map for CCD. The three mutational hot spot areas are shaded: CCD domain 1: 1–17; CCD domain 2: 39–46; CCD domain 3: 90–104. Missense mutations (closed circle) found in this study are shown at the top; previously reported mutations are indicated at the bottom. Open circle: recessive mutation; triangle: deletions; asterisk: mutations identified in this study but were also included in previous reports.

characteristic: these were ovoid in shape and with clearly demarcated borders, and were predominantly located in the centre of the fibres [60 ± 7% (mean ± SEM)]; they also occurred singly (98 ± 4%). In addition, most of the cores (72 ± 5%) in this group appeared to be 'rimmed' (Fig. 4B), which may connote high enzymatic activities around the cores on NADH-TR stain. More cores in type 1 fibres were also noted (90 ± 4%), but in general the percentage of the fibres with cores varied from 3 to 100%. No correlation was seen between clinical severity and the percentage of cores in fibres.

Some fibres show 'atypical' cores, characterized by indistinct borders and whose shapes were inexplicitly ovoid (Fig. 4E). These were seen more in non-C-terminal mutations but no statistical significance was observed as compared with C-terminal mutations (Fig. 3B). Like in typical core structures, these were also noted to be either in the centre of the fibre or in the subsarcolemmal areas.

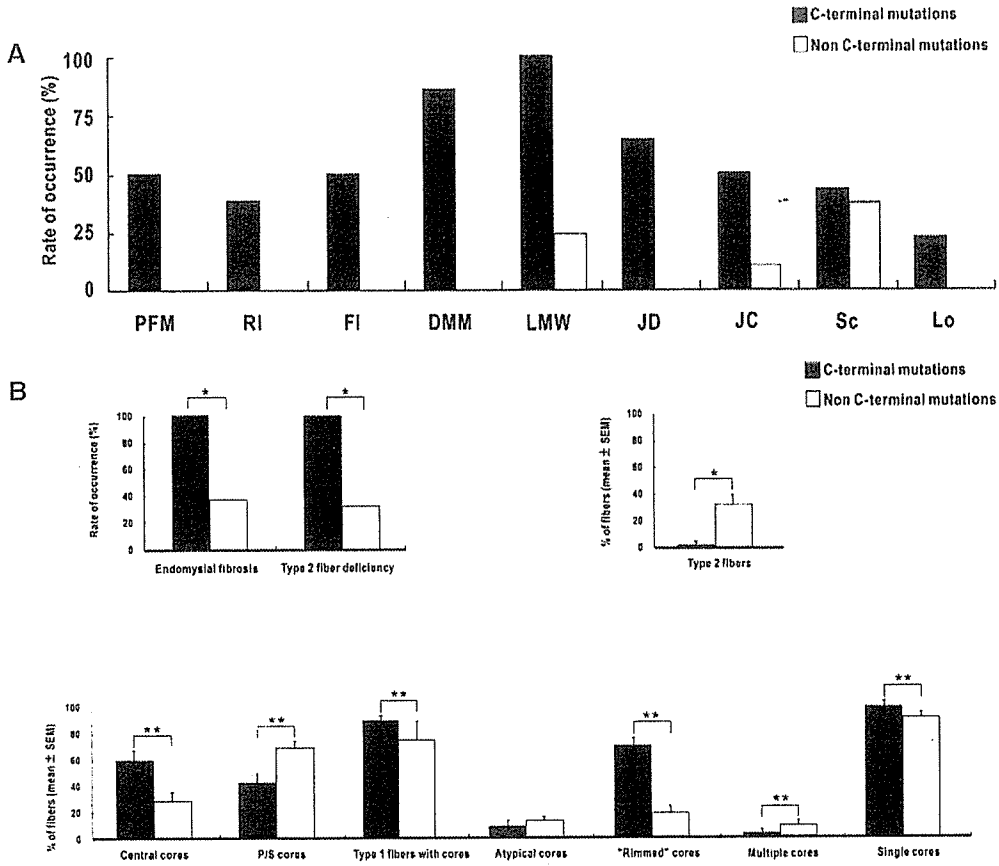

Fig. 3 (**A**) Genotype–phenotype correlation (clinical). Comparison of the clinical features between the patients with a heterozygous C-terminal mutation and those with a heterozygous non-C-terminal mutation. PFM = poor foetal movement; RI = respiratory insufficiency; FI = floppy infant; DMM = delayed motor milestone; JD = joint dislocation; JC = joint contracture; S = scoliosis; L = lordosis; LMW = limb muscle weakness. *$P < 0.05$, Fisher's exact test. (**B**) Genotype–phenotype correlation (pathological). Comparison of the pathological features between the patients with a heterozygous C-terminal mutation and those with a heterozygous non-C-terminal mutation. Note the characteristic endomysial fibrosis and fibre type 2 deficiency in patients with C-terminal mutations (upper panel). P/S = peripheral or subsarcolemmal. *$P < 0.05$, Fisher's exact test. **$P < 0.05$, Mann–Whitney test; SEM, standard error of means.

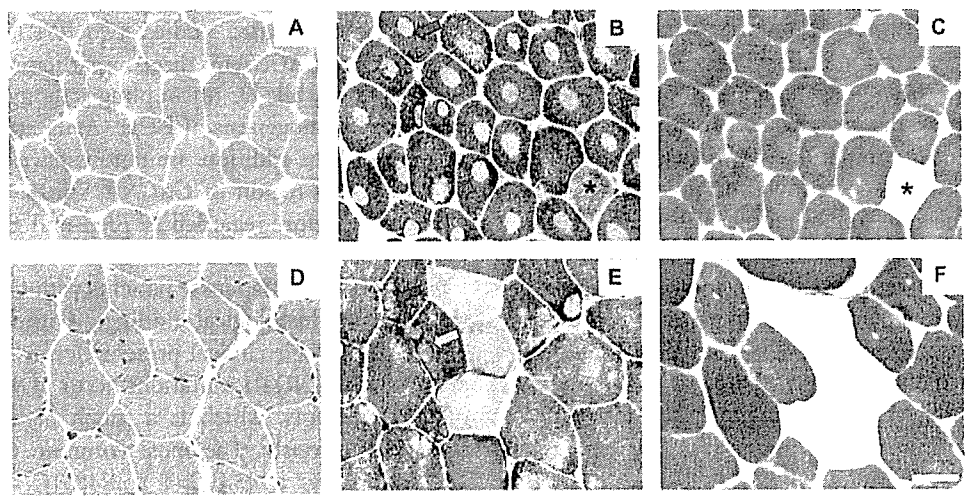

Fig. 4 Muscle biopsy. (**A–C**) A 9-year-old patient with a mutation in C-terminal region. (**A**) Minimal fibrosis is seen in mGT. (**B**) NADH-TR stain reveals the 'central core' in almost all fibres; note the 'rimming' of some cores (arrow). (**C**) Myosin ATPase staining, pH 4.4, clearly demonstrates type 2 fibre deficiency; type 2 fibre is marked with asterisk. (**D–F**) A 63-year-old patient with non-C-terminal mutation. (**D**) Minimal fibrosis is observed in mGT. (**E**) NADH shows cores but not on all type I fibres; note atypical cores (red arrow) and multiple cores in fibres (yellow arrow). (**F**) ATPase at pH 4.5 shows type 2 fibres in higher frequency compared with patient with C-terminal mutation. Bar denotes 50 microns.

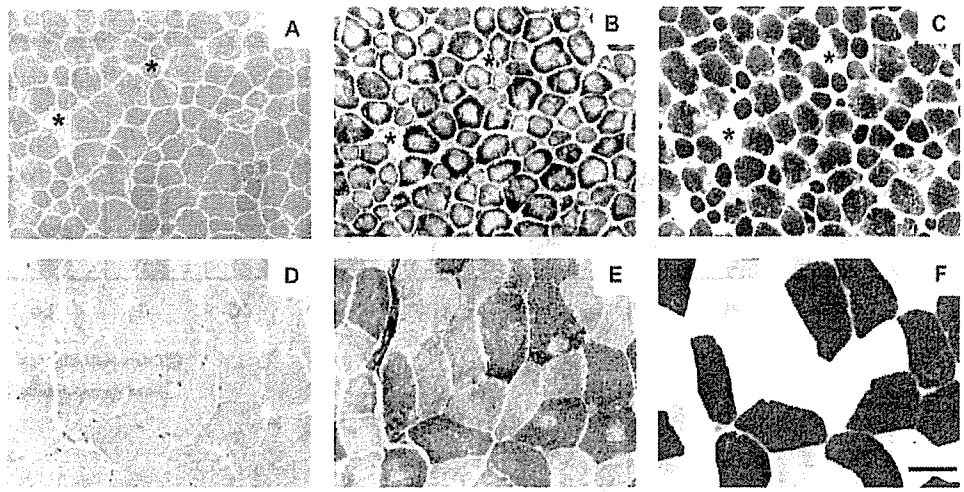

Fig. 5 Sections from patients in whom mutations were not found. (**A–C**) Sections from a 36-year-old female. (**A**) Moderate endomysial fibrosis is observed in mGT. (**B**) Cores are seen in almost all fibres; note that cores occupy the whole diameter of fibres, and the subsarcolemmal area surrounding the cores has high oxidative enzyme activity. (**C**) Type 2 fibre (asterisk) deficiency is seen in ATPase with pH 4.4 pre-incubation. (**A–C**) Biopsy findings from a 35-year-old female. (**D**) No endomysial fibrosis is noted in mGT. (**E**) Cores were seen but only in few type 1 fibres. (**F**) No fibre type 2 deficiency is observed (type 2 fibres comprised 72%). (**C**) Scale bar denotes 50 microns.

In Patients 1–8, from whom muscle biopsy was performed for CICR and cores were incidentally identified, all had non-C-terminal heterozygous mutations.

The clinical features of patients with two heterozygous mutations were more similar to those of the group with one heterozygous C-terminal mutation. In terms of muscle pathology, type 2 fibre deficiency was likewise seen (Table 2), similar to mutations involving the C-terminal region. This idea may also be buttressed by the fact that among a total of three patients with CRD, two carried a single C-terminal mutation, while the other had a compound heterozygous mutation. In terms of core pathology, however, they resemble that of non-C-terminal mutations: the cores were seen in 14 and 49% of type 1 fibres in Patients 24 and 25, respectively; and the characteristic 'rimming' of cores is less appreciated (Fig. 1).

In two patients in whom no mutation was found, the cores had peculiar features distinguishable from that seen in patients with identifiable mutations. Particularly, in Patient 26, the cores, albeit located centrally, occupied almost the whole diameter of the fibre, and, notably, the subsarcolemmal area around the cores had increased oxidative activity (Fig. 5). The cores in Patient 27 were initially considered to be regular cores but a closer look has shown that almost all the cores had indistinct borders; moreover, only <20% of type 1 fibres have cores (Fig. 5). In such cases, the term 'core-like' may be more appropriate to describe these structures.

Discussion

RYR1 mutations in CCD

At least 44 reported *RYR1* mutations have been associated with CCD, including 39 missense mutations and 5 deletions (Quane *et al.*, 1993; Zhang *et al.*, 1993; Fletcher *et al.*, 1995; Manning *et al.*, 1998; Lynch *et al.*, 1999; Monnier *et al.*, 2000, 2001; Avila and Dirksen, 2001; Tilgen *et al.*, 2001; Ferreiro *et al.*, 2002; Jungbluth *et al.*, 2002; Robinson *et al.*, 2002; Sewry *et al.*, 2002; Avila *et al.*, 2003*a*; Quinlivan *et al.*, 2003; Zorzato *et al.*, 2003; Shepherd *et al.*, 2004). All these mutations are clustered in the three 'hot spots', except for two (Fig. 2). *RYR1* mutations have been reported to be responsible for 47–67% of patients suffering from CCD, implying that the disease is genetically heterogeneous (Vainzof *et al.*, 2000; Monnier *et al.*, 2001). However, neither the true frequency nor the distribution of CCD-causative mutations has been accurately determined to date, since mutation screening has been limited to the three 'hot spots' of the *RYR1*, or even only to the C-terminal region. According to *in vitro* studies, two RYR1-binding proteins, *FKBP12* and *CACNA1S*, directly participate in or modulate EC coupling, while EC uncoupling is thought to be the linch-pin in the pathogenesis of CCD (Avila *et al.*, 2001; Lyfenko *et al.*, 2004). In addition, mutations have been identified in RYR1-binding region of *CACNA1S* in 1% of patients with MH. We therefore regarded *FKBP12* and *CACNA1S* genes as rational candidates for CCD.

We screened 27 Japanese patients with CCD, diagnosed on the basis of histological findings, without putting much emphasis on their clinical presentation as inclusion criteria, and found that *RYR1* mutations occur in 93% (25 out of 27) of CCD patients, which is a much higher rate than that thought previously. The most common CCD mutation in our cohort was c.14581C>T (p.R4861C). Interestingly, the c.14582G>A (p.R4861H) mutation that affects the same amino acid is the most common CCD mutation in European countries, while it was identified in only one patient from our series. Almost all reported patients bearing c.14582G>A had a positive family history, but all patients carrying mutation c.14581C>T were sporadic in this study and also in the

literature (Monnier *et al.*, 2001; Tilgen *et al.*, 2001; Davis *et al.*, 2003), suggesting that the 14 581 nucleotide might be susceptible to change.

To our knowledge, this is the first endeavour to screen the entire coding region of *RYR1* in a cohort of CCD patients. By screening the C-terminal region alone, we would have found *RYR1* mutations only in 59% (16 out of 27) of CCD patients, which is consistent with detection rates in previous reports, missing the two compound heterozygous mutations. Even extending the mutation screening to the three 'hot spots', we would have found *RYR1* mutations in only 67% (18 out of 27), also missing one compound heterozygous mutation. It thus becomes necessary to screen the entire *RYR1* coding region in CCD patients, however impractical it may be owing to the size of the gene. Interestingly, most of mutations outside the 'hot spots' were localized in exons 47 and 48, which neighbour the central region 'hot spot' (exons 39–46). Hence, mutation detection rate in CCD patients could be increased up to 89% by including exons 47 and 48, which may be a more practical alternative than sequencing the entire *RYR1* gene. In addition, *FKBP12* and *CACNA1S* may not be causative genes for CCD or an extremely rare, if they are, since there was no mutation in *FKBP12* or in the RYR1-binding region of *CACNA1S* genes.

We did not find any mutation in two patients in our cohort, suggesting that CCD may still be genetically heterogeneous even though there still remains the possibility that mutations may exist in unexamined regions, such as promoter region and introns, or that we may have overlooked a mutation. Notwithstanding this likelihood of other probabilities, the pathological characteristics of these patients are clearly different from the rest. If these patients were excluded from the analysis solely on the basis of the 'uncharacteristic' core-like structures, that is, if the inclusion criteria used were more stringent, the detection rate of mutations involving the *RYR1* gene will considerably and significantly increase to 100%.

Probable autosomal recessive CCD

CCD was once thought to be inherited solely via an autosomal dominant mechanism, but actually rare instances of recessive inheritance have also been identified (Manzur *et al.*, 1998; Ferreiro *et al.*, 2002; Romero *et al.*, 2003).

In this study, sequencing of the entire *RYR1* coding regions led to the identification of three patients (Patients 23, 24 and 25) with two heterozygous mutations. Patients 24 and 25 needed respiratory mechanical assistance after delivery, while their parents were completely healthy and without any skeletal abnormalities. In both patients, each of the two heterozygous mutations was, respectively, found in each of the parents, confirming that these patients had a compound heterozygous mutation. In Patient 25, p.R4893P affected the third residue of a very well conserved GVRAGGGIGD luminal motif (amino acids p.G4891-D4900) that has been proposed to be a pore-forming fragment responsible for the electrophysiological characteristics of the channel (Zhao *et al.*, 1999).

The parents of Patients 23 and 25 were asymptomatic, while they had heterozygous mutation, suggesting the recessive nature of these mutations. Since CCD patients could be clinically asymptomatic, however, we may not be able to completely exclude the possibility that their parents could have CCD. Nevertheless, judging from the clinical features and the mutation data, autosomal recessive mode of inheritance is most likely in these particular patients. Patient 24 also carried two heterozygous mutations (p.S427L in exon13, p.G4899E in exon 102), but further analysis was inevitably limited by the unavailability of samples from her parents, hampering full evaluation if this was indeed an autosomal recessive case. The p.G4899E mutation also affected the very well conserved GVRAGGGIGD luminal motif (G4899 underlined). Interestingly, this mutation has been reported in two papers as a causative heterozygous mutation (Monnier *et al.*, 2001; Romero *et al.*, 2003); however, since only the 'hot spots' were screened in these studies, the presence of another mutation is still possible and hence it might be impetuous to conclude that p.G4899E mutation is a causative dominant mutation.

Genotype–phenotype correlation

In general, CCD has a wide spectrum of phenotypic expression, ranging from the apparent absence of symptoms to the presence of perinatal complications and generalized muscle weakness. Mutations in the C-terminal region seem to be associated with certain clinical and pathological features: hypotonia during infancy, delayed motor development and limb muscle weakness; type 2 fibre deficiency and interstitial fibrosis; and characteristic cores with clearly demarcated borders, which are observed in almost all type 1 muscle fibres. In addition, 'rimming' on the borders of these cores is observed in much higher frequency; similarly, this phenomenon was also noted in the biopsy specimens of three families determined to have mutation in domain 3 (Sewry *et al.*, 2002). These unique features therefore delineate C-terminal mutations from other groups, at least in terms of muscle pathology.

In contrast, most of CCD patients harbouring at least one mutation outside the C-terminal region had only mild musculoskeletal abnormalities such as joint contractures and scoliosis. This phenomenon may be explained by the leaky-channel model and EC uncoupling model. Some non-C-terminal mutations in *RYR1* promote the leak of Ca^{2+} ions from the SR that may or may not be compensated by the activity of the sarco-endoplasmic reticulum Ca^{2+} ATPase (SERCA), resulting in an elevation of resting cytosolic Ca^{2+} and a depletion of SR Ca^{2+} stores. On the other hand, C-terminal mutations, especially those in the pore region of *RYR1*, may directly affect the channel gating properties, resulting in an abolition of orthograde activation by the

voltage-gated L-type Ca^{2+} channel or, in other words, EC uncoupling. However, there is no compensatory mechanism to increase Ca^{2+} release as SERCA pumps do in the leaky model (Tong *et al.*, 1999; Avila *et al.*, 2001, 2003*b*; Lyfenko *et al.*, 2004). This may explain why C-terminal mutations are associated with clinically evident muscle weakness.

Interestingly, all patients with enhanced CICR had a non-C-terminal heterozygous mutation. Although we did not measure CICR in patients with C-terminal mutations, our results may suggest that majority of CCD patients with MH susceptibility might have a non-C-terminal mutation, considering the facts that no patient with C-terminal mutation had a family history of MH susceptibility, and that one C-terminal mutation, p.I4898T, has been associated with normal halothane and caffeine sensitivities by an *in vitro* study (Lynch *et al.*, 1999). In a recent study made by Monnier *et al.* (2005), where individuals from IVCT-confirmed MH-susceptible families have been screened for *RYR1* mutations and CCD, some MH-normal patients had cores in type 1 fibres albeit the absence of mutation. It would thus be interesting to screen the whole *RYR1* in these patients, as only selected exons were included for genetic screening. In our study, however, we definitely cannot assume that patients with C-terminal mutations may have normal CICR test, as further evaluations are necessary. Furthermore, in only such patients, multiple cores were seen in addition to central cores. Thus, non-C-terminal heterozygous mutations may be more associated with multiple cores and MH susceptibility, although the number of patients is too small to enable us to draw a conclusion. Previous reports have asserted that exclusive MH susceptible patients have mutations in the C-terminal region, but there is only limited study on the histopathological evaluation of these patients, revealing the presence of cores; it is also important to stress that these cores are rather not characteristic of CCD (Ibarra *et al.*, 2006).

We have shown that the muscle pathology on the patients may differ among those with C-terminal mutations and those with mutations outside this area. Cores, moreover, were not only located in the centre of the muscle fibres but also in subsarcolemmal or peripheral areas, and atypical cores can also be seen in such cases, indicating that the possibility of *RYR1* mutation cannot be excluded in patients with such atypical cores. Here, atypical cores of CCD were still different from the cores of MmD, for most of the cores were clearly demarcated and only some fibres appeared to have more than one core; nevertheless, histological, clinical, genetic features and mode of inheritance overlap between CCD and MmD, making the boundary of these two diseases blurred (Lyfenko *et al.*, 2004; Mathews *et al.*, 2004). Patients 24 and 25, who possessed double mutations, had pathology akin to characteristics of both C- and non-C-terminal mutations: type 2 fibre deficiency is seen, and cores are rather atypical and are only seen in moderate number on type 1 fibres. This may, in part, be explained by the fact that these patients carry mutations in and outside the C-terminal region.

In the past, we may have been biased in interpreting the phenotype–genotype correlation between CCD and *RYR1* mutations, since mutation screening had been limited to the 'hot spots'. Quane *et al.* (1993) claimed that various phenotypes could be observed even among patients with the same mutation. However, their patients may have had a compound heterozygous mutation and one of the mutations may have been overlooked. In fact, if we had just screened the *RYR1* C-terminal region of patients with two heterozygous mutations (Patients 24 and 25), we would have found only one mutation, giving an impression of remarkable phenotypic difference between the patients and their healthy parents, regardless of the presence of the same 'heterozygous' mutation.

In summary, our comprehensive mutation screening revealed a surprisingly higher detection rate of *RYR1* mutations in CCD patients than that revealed in previous reports, which accounts for >90% of the cases. Our results also suggest the possibility that many *RYR1* mutations may have been overlooked by the regularly used screening methods that cover only three 'hot spots'. At least, exons 47 and 48 should be included into the hot spot screening if a comprehensive mutation analysis of *RYR1* is not feasible. In terms of muscle pathology, patients with mutations involving the C-terminal region have characteristic cores that can be easily distinguished from those with mutations outside this domain, and also from those patients without mutation in the *RYR1*. Needless to say, the pathomechanism of how these cores develop still remains to be elucidated.

Acknowledgements

The authors thank the patients, their family and physicians for their cooperation. This study is supported partly by the 'Research on Health Sciences focusing on Drug Innovation' from the Japanese Health Sciences Foundation; partly by the 'Research on Psychiatric and Neurological Diseases and Mental Health' of 'Health and Labour Sciences Research Grants' and the 'Research Grant (17A-10) for Nervous and Mental Disorders', from the Ministry of Health, Labour and Welfare; partly by the 'Grant-in-Aid for Scientific Research' from the Japan Society for the Promotion of Science; and partly by the 'Program for Promotion of Fundamental Studies in Health Sciences' of the National Institute of Biomedical Innovation (NIBIO).

References

Avila G, Dirksen RT. Functional effects of central core disease mutations in the cytoplasmic region of the skeletal muscle ryanodine receptor. J Gen Physiol 2001; 118: 277–90.

Avila G, O'Brien J, Dirksen RT. Excitation-contraction uncoupling by a human central core disease mutation in the ryanodine receptor. Proc Natl Acad Sci USA 2001; 98: 4215–20.

Avila G, O'Connell KM, Dirksen RT. The pore region of the skeletal muscle ryanodine receptor is a primary locus for excitation-contraction uncoupling in central core disease. J Gen Physiol 2003a; 121: 277–86.

Avila G, Lee E, Perez CF, Allen PD, Dirksen RT. FKBP12 binding to *RYR1* modulates excitation-contraction coupling in mouse skeletal myotubes. J Biol Chem 2003b; 278; 22600–8.

Balshaw D, Gao L, Meissner G. Luminal loop of the ryanodine receptor: a pore-forming segment? Proc Natl Acad Sci USA 1999; 96: 3345–7.

Davis MR, Haan E, Jungbluth H, Sewry C, North K, Muntoni F, et al. Principal mutation hotspot for central core disease and related myopathies in the C-terminal transmembrane region of the *RYR1* gene. Neuromuscul Disord 2003; 13: 151–7.

Ferreiro A, Monnier N, Romero NB, Leroy JP, Bonnemann C, Haenggeli CA, et al. A recessive form of central core disease, transiently presenting as multi-minicore disease, is associated with a homozygous mutation in the ryanodine receptor type 1 gene. Ann Neurol 2002; 51: 750–9.

Fletcher JE, Tripolitis L, Hubert M, Vita GM, Levitt RC, Rosenberg H. Genotype and phenotype relationships for mutations in the ryanodine receptor in patients referred for diagnosis of malignant hyperthermia. Br J Anaesth 1995; 75: 307–10.

Ibarra M CA, Ichihara Y, Hikita M, Yoshida K, Junji S, Maehara Y, et al. Effect of bupivacaine enantiomers on Ca^{2+} release from sarcoplasmic reticulum in skeletal muscle. Eur J Pharmacol 2005; 512: 77–83.

Ibarra M CA, Wu S, Murayama K, Minami N, Ichihara Y, Kikuchi H, et al. Malignant hyperthermia in Japan: mutation screening of the entire ryanodine receptor type 1 gene coding region by direct sequencing. Anesthesiology 2006. In press.

Jungbluth H, Muller CR, Halliger-Keller B, Brockington M, Brown SC, Feng L, et al. Autosomal recessive inheritance of *RYR1* mutations in a congenital myopathy with cores. Neurology 2002; 59: 284–7.

Leong P, MacLennan DH. The cytoplasmic loops between domains II and III and domains III and IV in the skeletal muscle dihydropyridine receptor bind to a contiguous site in the skeletal muscle ryanodine receptor. J Biol Chem 1998; 273: 29958–64.

Lorenzon NM, Beam KG. Calcium channelopathies. Kidney Int 2000; 57: 794–802.

Lyfenko AD, Goonasekera SA, Dirksen RT. Dynamic alterations in myoplasmic Ca^{2+} in malignant hyperthermia and central core disease. Biochem Biophys Res Commun 2004; 322: 1256–66.

Lynch PJ, Tong J, Lehane M, Mallet A, Giblin L, Heffron JJ, et al. A mutation in the transmembrane/luminal domain of the ryanodine receptor is associated with abnormal Ca^{2+} release channel function and severe central core disease. Proc Natl Acad Sci USA 1999; 96: 4164–9.

Magee KR, Shy GM. A new congenital non-progressive myopathy. Brain 1956; 79: 610–21.

Manning BM, Quane KA, Ording H, Urwyler A, Tegazzin V, Lehane M, et al. Identification of novel mutations in the ryanodine-receptor gene (*RYR1*) in malignant hyperthermia: genotype–phenotype correlation. Am J Hum Genet 1998; 62: 599–609.

Manzur AY, Sewry CA, Ziprin J, Dubowitz V, Muntoni F. A severe clinical and pathological variant of central core disease with possible autosomal recessive inheritance. Neuromuscul Disord 1998; 8: 467–73.

Mathews KD, Moore SA. Multiminicore myopathy, central core disease, malignant hyperthermia susceptibility, and RYR1 mutations: one disease with many faces? Arch Neurol 2004; 61: 27–9.

McCarthy TV, Quane KA, Lynch PJ. Ryanodine receptor mutations in malignant hyperthermia and central core disease. Hum Mutat 2000; 15: 410–7.

Monnier N, Romero NB, Lerale J, Nivoche Y, Qi D, MacLennan DH, et al. An autosomal dominant congenital myopathy with cores and rods is associated with a neomutation in the RYR1 gene encoding the skeletal muscle ryanodine receptor. Hum Mol Genet 2000; 9: 2599–608.

Monnier N, Romero NB, Lerale J, Landrieu P, Nivoche Y, Fardeau M, et al. Familial and sporadic forms of central core disease are associated with mutations in the C-terminal domain of the skeletal muscle ryanodine receptor. Hum Mol Genet 2001; 10: 2581–92.

Monnier N, Kozak-Ribbens G, Krivosic-Horber R, Nivoche Y, Qi D, Kraev N, et al. Correlations between genotype and pharmacological, histological, functional, and clinical phenotypes in malignant hyperthermia susceptibility. Hum Mutat 2005; 26: 413–25.

Quane KA, Healy JM, Keating KE, Manning BM, Couch FJ, Palmucci LM, et al. Mutations in the ryanodine receptor gene in central core disease and malignant hyperthermia. Nat Genet 1993; 5: 51–5.

Quinlivan RM, Muller CR, Davis M, Laing NG, Evans GA, Dwyer J, et al. Central core disease: clinical, pathological, and genetic features. Arch Dis Child 2003; 88: 1051–5.

Robinson RL, Brooks C, Brown SL, Ellis FR, Halsall PJ, Quinnell RJ, et al. *RYR1* mutations causing central core disease are associated with more severe malignant hyperthermia in vitro contracture test phenotypes. Hum Mutat 2002; 20: 88–97.

Romero NB, Monnier N, Viollet L, Cortey A, Chevallay M, Leroy JP, et al. Dominant and recessive central core disease associated with *RYR1* mutations and fetal akinesia. Brain 2003; 126: 2341–9.

Sambrook J, Russell DW. Molecular cloning: a laboratory manual. Cold Spring Harbor, NY: Cold Spring Harbor Laboratory Press; 2001.

Sewry CA, Muller C, Davis M, Dwyer JS, Dove J, Evans G, et al. The spectrum of pathology in central core disease. Neuromuscul Disord 2002; 12: 930–8.

Shepherd S, Ellis F, Halsall J, Hopkins P, Robinson R. *RYR1* mutations in UK central core disease patients: more than just the C-terminal transmembrane region of the *RYR1* gene. J Med Genet 2004; 41: e33

Shuaib A, Paasuke RT, Brownell KW. Central core disease. Clinical features in 13 patients. Medicine (Baltimore) 1987; 66: 389–96.

Stewart SL, Hogan K, Rosenberg H, Fletcher JE. Identification of the Arg1086His mutation in the alpha subunit of the voltage-dependent calcium channel (CACNA1S) in a North American family with malignant hyperthermia. Clin Genet 2001; 59: 178–84.

Tilgen N, Zorzato F, Halliger-Keller B, Muntoni F, Sewry C, Palmucci LM, et al. Identification of four novel mutations in the C-terminal membrane spanning domain of the ryanodine receptor 1: association with central core disease and alteration of calcium homeostasis. Hum Mol Genet 2001; 10: 2879–87.

Tong J, McCarthy TV, MacLennan DH. Measurement of resting cytosolic Ca^{2+} concentrations and Ca^{2+} store size in HEK-293 cells transfected with malignant hyperthermia or central core disease mutant Ca^{2+} release channels. J Biol Chem 1999; 274: 693–702.

Treves S, Anderson AA, Ducreux S, Divet A, Bleunven C, Grasso C, et al. Ryanodine receptor 1 mutations, dysregulation of calcium homeostasis and neuromuscular disorders. Neuromuscul Disord 2005; 15: 577–87.

Vainzof M, Muniz VP, Tsanaclis AM, Silva HC, Rusticci MS. Does the A3333G mutation in the CACNL1A3 gene, detected in malignant hyperthermia, also occur in central core disease? Genet Test 2000; 4: 383–6.

Weiss RG, O'Connell KM, Flucher BE, Allen PD, Grabner M, Dirksen RT. Function analysis of the R1086H malignant hyperthermia mutation in the DHPR reveals an unexpected influence of the III-IV loop on skeletal muscle EC coupling. Am J Physiol Cell Physiol 2004; 287: 1094–102.

Zhang Y, Chen HS, Khanna VK, De Leon S, Phillips MS, Schappert K, et al. A mutation in the human ryanodine receptor gene associated with central core disease. Nat Genet 1993; 5: 46–50.

Zhao M, Li P, Li X, Zhang L, Winkfein RJ, Chen SR. Molecular identification of the ryanodine receptor pore-forming segment. J Biol Chem 1999; 274: 25971–4.

Zorzato F, Yamaguchi N, Xu L, Meissner G, Muller CR, Pouliquin P, et al. Clinical and functional effects of a deletion in a COOH-terminal lumenal loop of the skeletal muscle ryanodine receptor. Hum Mol Genet 2003; 12: 379–88.

Human Molecular Genetics, 2007, Vol. 16, No. 2 *115–128*
doi:10.1093/hmg/ddl446
Advance Access published on December 12, 2006

A *Gne* knockout mouse expressing human V572L mutation develops features similar to distal myopathy with rimmed vacuoles or hereditary inclusion body myopathy

May Christine V. Malicdan, Satoru Noguchi*, Ikuya Nonaka, Yukiko K. Hayashi and Ichizo Nishino

Department of Neuromuscular Research, National Institute of Neuroscience, National Center of Neurology and Psychiatry, 4-1-1 Ogawahigashi-cho, Kodaira, Tokyo 187-8502, Japan

Received October 3, 2006; Revised November 2, 2006; Accepted November 21, 2006

Distal myopathy with rimmed vacuoles (DMRV) or hereditary inclusion myopathy (h-IBM) is an early adult-onset distal myopathy caused by mutations in the UDP-*N*-acetylglucosamine 2-epimerase/*N*-acetylmannosamine kinase (*GNE*) gene which encodes for a bifunctional enzyme involved in sialic acid biosynthesis. It is pathologically characterized by the presence of rimmed vacuoles especially in atrophic fibers, which also occasionally contain congophilic materials that are immunoreactive to β-amyloid, lysosomal proteins, ubiquitin and tau proteins. To elucidate the pathomechanism of this myopathy and to explore the treatment options, we generated a mouse model of DMRV/h-IBM. We knocked out the *Gne* gene in the mouse, but this resulted in embryonic lethality. We therefore generated a transgenic mouse that expressed the human *GNE*V572L mutation, which is the most prevalent among Japanese DMRV patients, and crossed this with $Gne^{(+/-)}$ mouse to obtain $Gne^{(-/-)}$h*GNE*V572L-Tg. Interestingly, these mice exhibit marked hyposialylation in serum, muscle and other organs. Reduction in motor performance in these mice can only be seen from 30 weeks of age. A compelling finding is the development of β-amyloid deposition in myofibers by 32 weeks, which clearly precedes rimmed vacuole formation at 42 weeks. These results show that the $Gne^{(-/-)}$ h*GNE*V572L-Tg mouse mimics the clinical, histopathological and biochemical features of DMRV/h-IBM, making it useful for understanding the pathomechanism of this myopathy and for employing different strategies for therapy. Our findings underscore the notion that hyposialylation plays an important role in the pathomechanism of DMRV/h-IBM.

INTRODUCTION

Distal myopathy with rimmed vacuoles (DMRV) is an autosomal recessive myopathy which was originally reported by Nonaka *et al.*, (1) thus it is also known as Nonaka myopathy. It is the same entity with hereditary inclusion body myopathy (h-IBM), which was initially reported among Iranian Jews (2). DMRV/h-IBM usually starts affecting adults from ages 15 to 40 years with an average onset of 26 years and with an initial symptom of altered gait (1). It is gradually progressive, and patients become wheelchair-bound between 26 and 57 years of age, or about an average of 12 years after the onset of symptoms (3).

DMRV/h-IBM is characterized by preferential involvement of the distal muscles of lower extremities especially the tibialis anterior muscles, with relative sparing of the quadriceps, hence the term 'quadriceps-sparing' rimmed vacuolar myopathy (2). Other muscles are involved as well, especially late in the course of the disease (3). Serum creatine kinase (CK) level is normal or mildly elevated. The characteristic finding on muscle biopsy is the presence of rimmed vacuoles (RVs), which are actually empty spaces surrounded by aggregation of autophagic vacuoles. These RVs occasionally contain congophilic materials that are immunoreactive to various proteins, including amyloid β, phosphorylated tau, ubiquitin and

*To whom correspondence should be addressed. Tel: +81 423461712; Fax: +81 423461742; Email: noguchi@ncnp.go.jp

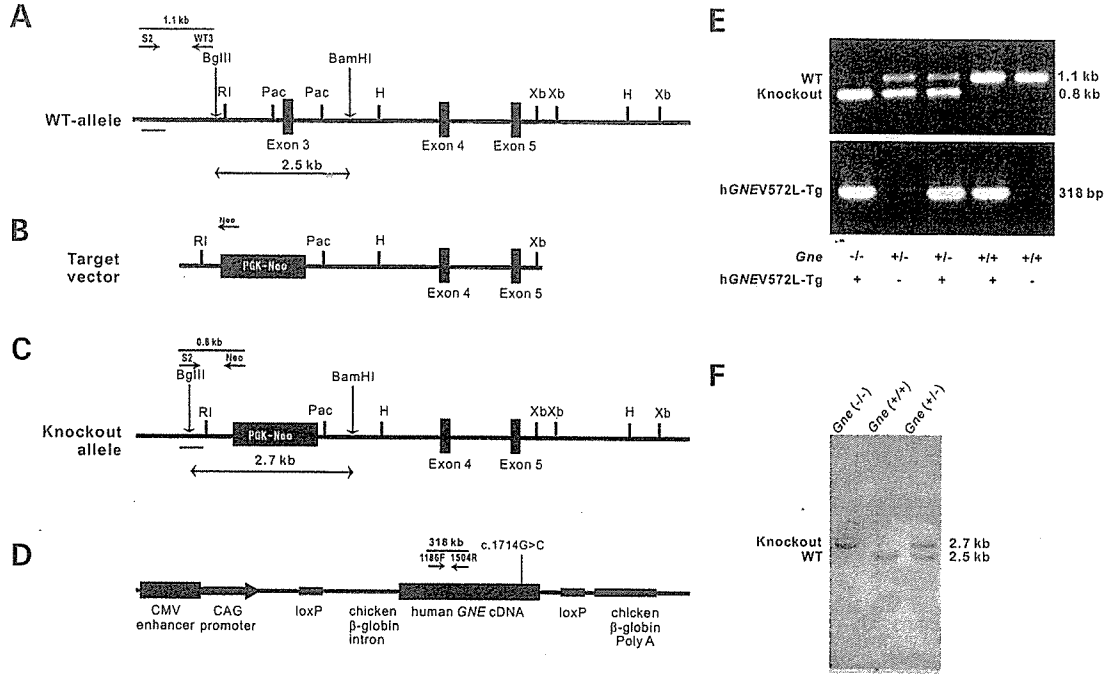

Figure 1. Genomic configuration of the *Gne* gene and targeting vector. Schematic structure of the WT *Gne* gene (**A**), which contains exon 3–5. Positions of restriction enzyme sites are shown. H, *Hin*dIII; Pac, *Pac*I; RI, *Eco*RI; Xb, *Xba*I. A 10.5 kb *Eco*RI–*Xba*I fragment was subcloned to make the targeting vector (**B**). One side of the Neo cassette was inserted 1.4 kb upstream of exon 3, and the other side of which was inserted 124 bp downstream of exon 3. In the knockout allele (**C**), the Neo cassette replaced the 1.4 kb upstream of exon 3, exon 3 and 124 bp downstream of exon 3. We selected homologous recombinants by neomycin resistance. (**D**) Structure of mutated human *GNE*V572L construct. CAG promoter was used to achieve expression in various tissues. (**E**) Genotyping of *Gne* and h*GNE*V572L-Tg mice by PCR. Five genotypes resulting from crossing a $Gne^{(+/-)}$h*GNE*V572L-Tg and $Gne^{(+/-)}$ are shown [from left to right: $Gne^{(-/-)}$ h*GNE*V572L-Tg (+); $Gne^{(+/-)}$h*GNE*V572L-Tg(−); $Gne^{(+/-)}$h*GNE*V572L-Tg(−); $Gne^{(+/+)}$h*GNE*V572L-Tg(+); and $Gne^{(+/+)}$h*GNE*V572L-Tg(−)]. In *Gne* genotyping (upper panel), the 0.8 and 1.1 kb bands represent knockout and WT alleles, respectively [PCR products amplified by primer sets are illustrated in (A) and (C)]. In h*GNE*V572L-Tg genotyping (lower panel), the presence of 318 bp band represents the integration of the h*GNE*V572L transgene. (**F**) Confirmation of *Gne* genotypes by Southern blot analysis. Tail genomic DNA were digested with *Bgl*II and *Bam*HI and analyzed by Southern blot analyses with 5′ probes shown as bars in (A) and (C). The fragments of 2.7 and 2.5 kb represent knockout and WT alleles, respectively.

α-synuclein. Necrotic and regenerating fibers and areas of inflammation are uncommon but can be seen. Ultrastructurally, filamentous inclusions measuring 18–20 nm in diameter are seen in both the cytoplasm and nucleus (3), in addition to the presence of autophagy and various inclusions.

DMRV/h-IBM was mapped to chromosome 9 (4,5), and was shown to be associated with mutations in the *GNE* gene (6,7), which encodes for a bifunctional enzyme that catalyzes the rate-limiting step in sialic acid biosynthesis (8). All patients acquire the disease by autosomal recessive pattern, and have at least one missense mutation in one allele, including the most common mutations V572L and M712T among Japanese and Iranian Jews, respectively. No patient with homozygous null mutation was identified. Genetically confirmed DMRV/h-IBM diseases, initially recognized among Japanese and Iranian Jews (6,9–11), appear to afflict patients with diverse nationalities and cultural backgrounds (12–16).

The mechanism by which mutations in the *GNE* lead to the phenotype in DMRV/h-IBM has remained unclear. We previously demonstrated that mutations in the *GNE* led to the reduction in either the UDP-GlcNAc 2-epimerase or ManNAc kinase activity (17); moreover, we have shown that myotubes from DMRV patients are hyposialylated, and this phenomenon can be corrected by the addition of free sialic acid and/or its precursor. Other groups have shown similar results regarding GNE activity, but in contrast, they suggested that only the cells derived from a patient carrying a homozygous epimerase mutation had a significant reduction in the overall membrane-bound sialic acid (18), and that *GNE* mutations may not contribute to alteration in sialylation in h-IBM myoblasts (19). To address these issues, we developed a mouse model for the disease. In this article, we present the first DMRV/h-IBM mouse model that expressed only the mutated human *GNE* and show that this mouse evidently displays features of DMRV/h-IBM seen in human patients.

RESULTS

Production of $Gne^{(-/-)}$h*GNE*V572L-Tg

In Figure 1, the genomic configuration of the *Gne* gene (A) and the targeting construct (B) are shown. The inserted Neo cassette replaced the 1.4 kb upstream of exon 3, exon 3 and 1.4 kb downstream of exon 3. Only WT and $Gne^{(+/-)}$ mice were generated; no $Gne^{(-/-)}$ mouse was produced (data not shown), in concurrence with a previous report (20). We then proceeded to generate a transgenic mouse (h*GNE*V572L-Tg) that expressed the human mutated *GNE* with V572L, the most common *GNE* mutation in Japan, the structure of which is shown in Figure 1D. Of the resulting litters, nine

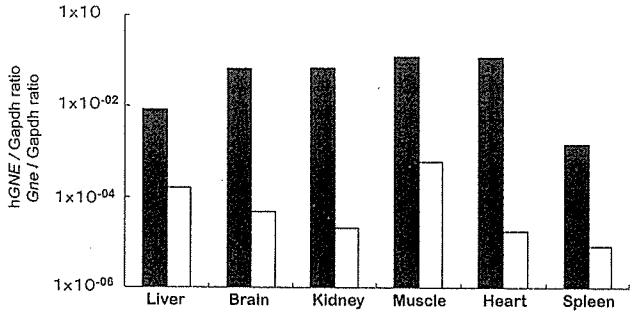

Figure 2. Expression of h*GNE*V572L (closed bars) and endogenous *Gne* (open bars) relative to Gapdh. Log-values were used for computation of ratio. Highest expression of h*GNE*V572L is seen in skeletal and cardiac muscles, followed by heart, kidney, brain, liver and spleen.

mice were found to incorporate the h*GNE*V572L by PCR analysis of genomic DNA isolated from tail snips, but only four lines were able to generate offspring. Using quantitative RT-PCR, we quantified mRNA expression of h*GNE*V572L and endogenous *Gne* in muscle and other organs of these transgenic mice. Transgene expression was highest in the skeletal muscle, followed by heart, kidney, brain, spleen and liver (Fig. 2), while endogenous *Gne* expression was barely detected. We also determined the copy number using quantitative PCR by comparing the amplification of h*GNE*V572L with endogenous *Gne*. We calculated the copy numbers for lines 3, 6, 7 and 9 as 2, 4, 3 and 5, respectively. Consequently, we used this transgenic line 9 for producing the model mouse.

We crossed the h*GNE*V572L transgenic mouse with a $Gne^{(+/-)}$ to obtain a $Gne^{(+/-)}$h*GNE*V572L-Tg. Further, we crossed this $Gne^{(+/-)}$h*GNE*V572L-Tg with a $Gne^{(+/-)}$ to generate our model mouse, a transgenic mouse on a *Gne* knockout background, $Gne^{(-/-)}$h*GNE*V572L-Tg. Analysis of 823 newborn mice from independent heterozygous crosses indicated that the numbers of mice with the five genotypes, $Gne^{(-/-)}$h*GNE*V572L-Tg (+), $Gne^{(+/-)}$h*GNE*V572L-Tg(+), $Gne^{(+/-)}$h*GNE*V572L-Tg(−), $Gne^{(+/+)}$h*GNE*V572L-Tg(+) and $Gne^{(+/+)}$h*GNE*V572L-Tg(−) were 72 (9%), 225 (28%), 193 (24%), 177 (22%) and 136 (17%), respectively, almost approximating the expected ratio of Mendelian inheritance. Mice of the latter four genotypes did not demonstrate unusual phenotype, and thus were considered as control littermates. Images for routine PCR for checking *Gne* genotype and the incorporation of the human *GNE*V572L are shown in Figure 1E, with the corresponding PCR fragments illustrated in A, C and D.

Hyposialylation is evident in the $Gne^{(-/-)}$h*GNE*V572L-Tg

Understandably, mutations in the *GNE* can affect sialylation of glycoconjugates because of the gene's role in sialic acid synthesis. We therefore measured the sialic acid levels in the $Gne^{(-/-)}$h*GNE*V572L-Tg mice using HPLC with fluorometric detection. In wild-type (WT) mice, sialic acid levels are highest in the brain, followed by the liver, spleen and kidney (Fig. 3B, open boxes). In both skeletal and cardiac muscles, sialic acid levels are evidently lower than in other tissues. As we have expected, the total sialic acid in the $Gne^{(-/-)}$h*GNE*V572L-Tg mice is remarkably lower than WT. This hyposialylation is most remarkable in the serum (Fig. 3A). A significant reduction in total sialic acid level is seen in various tissues examined (Fig. 3B, closed boxes). We also measured sialic acid level in the h*GNE*V572L-Tg and noted that sialic acid levels are comparable with WT mice (Fig. 3B, gray boxes), although the transgenic expression was extremely higher than endogenous *GNE*.

$Gne^{(-/-)}$h*GNE*V572L-Tg has lower median of survival than littermate

The $Gne^{(-/-)}$h*GNE*V572L-Tg mice were indistinguishable from their littermates at birth and seemed healthy (Fig. 4A and B). After 30 weeks of age, these mice weighed less than their littermates (Fig. 4). Significant difference in weight is more pronounced and earlier in female $Gne^{(-/-)}$ h*GNE*V572L-Tg (Fig. 4C) mice when compared with male (Fig. 4D). To investigate plausible explanations for this difference in weight, we performed gross inspection of the muscles, and found out that some muscles, especially the gastrocnemius, were atrophic in the $Gne^{(-/-)}$h*GNE*V572L-Tg when compared with control (Fig. 4E and F), and this finding was more remarkable among females (Fig. 4E).

Surprisingly, the median survival rate were lower in the $Gne^{(-/-)}$h*GNE*V572L-Tg as seen in Figure 4B. The cause of death could not be ascertained, but upon necropsy, no external gross abnormalities were seen and the internal organs appeared normal. On pathological examination, five out of 12 (41%) mice that died had RVs in the skeletal muscle; among these five mice, only one was before 40 weeks of age. Twenty five percent had fibrosis and a few RVs in the diaphragm. Thirty-three percent had fibrosis in the cardiac muscles.

$Gne^{(-/-)}$h*GNE*V572l-Tg shows clinical phenotype

Using a tool for assessing general muscle strength, these mice notably performed worse than their littermates (Fig. 5A). Interestingly, significant change in muscle power is noted after 30 weeks of age. We then proceeded to measure serum CK activity in the mice and found out that CK was significantly elevated in the $Gne^{(-/-)}$h*GNE*V572L-Tg mice when compared with their littermates (Fig. 5B), albeit the observation that these values are much lower when compared with muscular dystrophy models like $Large^{myd}$ and $Sgcb^{(-/-)}$ mice (data not shown). Because the appearance of phenotype seemed to be related to age, we measured CK activity according to different age groups. From Figure 5C, we note that elevation of CK activity starts at 30 weeks of age. Using gel electrophoresis, we verified that CK-MM isozyme was primarily increased (data not shown).

$Gne^{(-/-)}$h*GNE*V572l-Tg shows characteristic pathological features of DMRV

We checked if the $Gne^{(-/-)}$h*GNE*V572L-Tg mice showed muscle phenotype not only by the analysis of muscle power

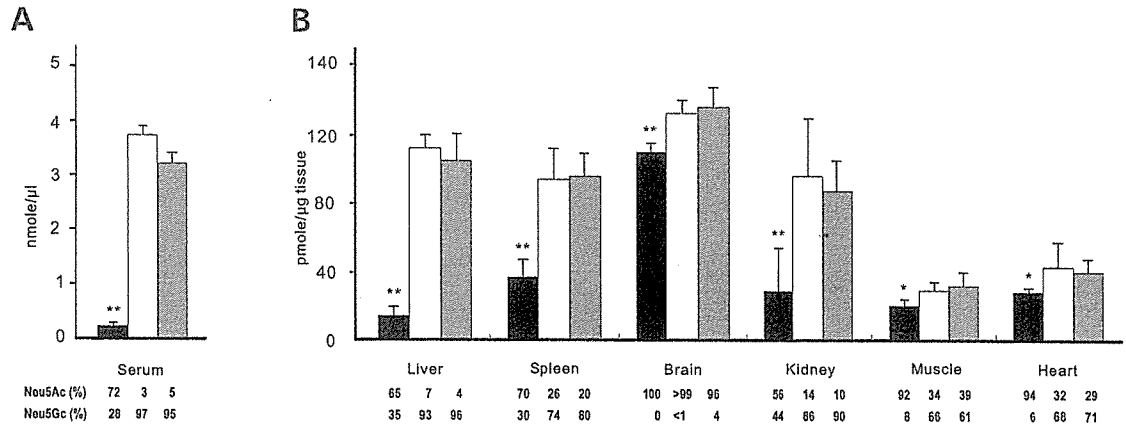

Figure 3. Measurement of total sialic acid in serum (**A**) and tissues (**B**) in $Gne^{(-/-)}$h*GNE*V572L-Tg (closed bars), WT (open bars) and h*GNE*V572L-Tg (gray bars); bars represent mean total sialic acid level with SD. Breakdown of sialic acid contents according to standards used (Neu5Ac and Neu5Gc) are shown below. Sialic acid levels of WT and h*GNE*V572L-Tg are comparable. Note the reduction of sialic acid levels in the serum and tissues of the $Gne^{(-/-)}$h*GNE*V572L-Tg mice. Single asterisk, $P < 0.05$; double asterisks, $P < 0.005$.

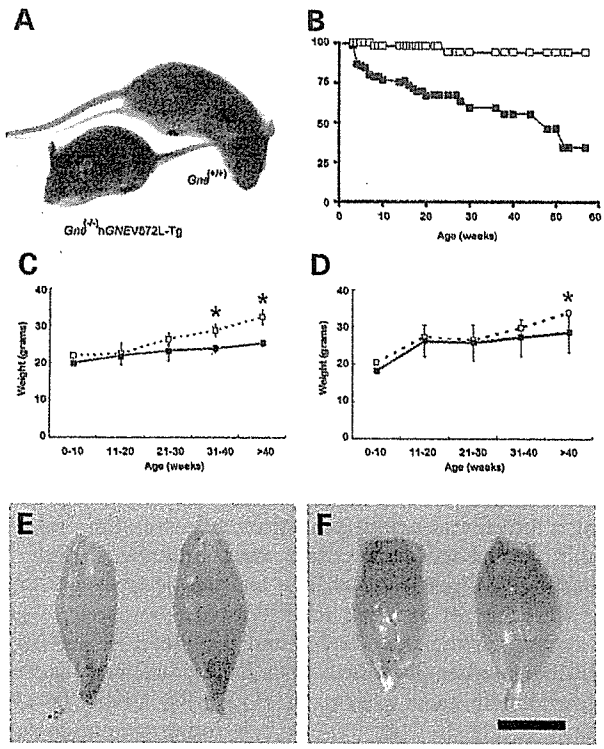

Figure 4. Overall phenotype of the $Gne^{(-/-)}$h*GNE*V572L-Tg mice. (**A**) Picture of WT (up) and $Gne^{(-/-)}$h*GNE*V572L-Tg (down) at 16 weeks of age. (**B**) Survival curve of mice: WT (open squares, $n = 71$ for males and females), $Gne^{(-/-)}$h*GNE*V572L-Tg mice (closed squares, $n = 71$ for males and females). $Gne^{(-/-)}$h*GNE*V572L-Tg mice have significantly reduced life spans when compared with WT mice (log-rank test: $P = 0.001$). (**C**) Growth curves of female: WT (open squares, $n = 10$ per age group), $Gne^{(-/-)}$h*GNE*V572L-Tg mice (closed squares, $n = 10$ per age group) (**D**) Growth curves of male mice: WT (open squares, $n = 10$ per age group), $Gne^{(-/-)}$h*GNE*V572L-Tg (closed squares, $n = 10$ per age group). $Gne^{(-/-)}$h*GNE*V572L-Tg mice have lower body weight after 30 weeks of age, and this is more pronounced in females; asterisk denotes $P < 0.05$, Mann–Whitney U test. Gastrocnemius muscles of female (**E**) and male (**F**) mice: $Gne^{(-/-)}$h*GNE*V572L-Tg (left) and littermate (right). Atrophy is noted on gross inspection of h*GNE*V572L-Tg gastrocnemius muscles; bar represents 5 mM.

but also by evaluating biopsy samples in five different age groups (10, 20, 30, 40 and 50 weeks). Morphometric analysis of the fibers in different age groups showed that the variation in fiber size becomes more marked with age, preferentially affecting the gastrocnemius and quadriceps muscles (data not shown); for this reason, we used the gastrocnemius muscle in further experiments. We found that at young age, they developed neither clinical nor pathological phenotype, as they were comparable with WT. Figure 6A, D and G shows representative sections from the $Gne^{(-/-)}$h*GNE*V572L-Tg mice per age group. Histopathological analysis revealed almost normal findings in the muscle sections before 30 weeks of age (data not shown). In general, necrotic and regenerating processes are not observed in the young mice, although a few necrotic fibers are observed as they grow older. No endomysial or perimysial inflammation is seen.

Scattered small angular fibers are noted by 30 weeks of age (Fig. 6A), which is not seen in the littermates (Fig. 6B and C). The variation in fiber size becomes more noticeable as the mice grow older. In addition, fibers appear atrophic by 40 weeks of age, in support with the observation that the gastrocnemius muscle is relatively atrophic by gross inspection. Remarkably after 40 weeks, RVs are seen in scattered fibers (arrows in Fig. 6D and G). Occasionally, inclusion bodies are found in the fibers with or without RVs (arrowhead in Fig. 7A and B). Like in humans, these RVs are intensely stained with acid phosphatase, giving the impression that autophagic process is activated (Fig. 7C). We confirmed this by checking the expression of lysosomal-associated proteins (LAMPs) 1 and 2, and LC3 in muscle sections, all of which are upregulated. LAMP-1 is predominantly expressed within the vicinity of RVs (Fig. 7E). LAMP-2, on the other hand, noticeably is also expressed in the subsarcolemmal areas aside from its localization in the area of RVs (Fig. 7F). LC3 immunoreactivity is almost similar to LAMP-2, except that the perinuclear region is also highlighted (Fig. 7G).

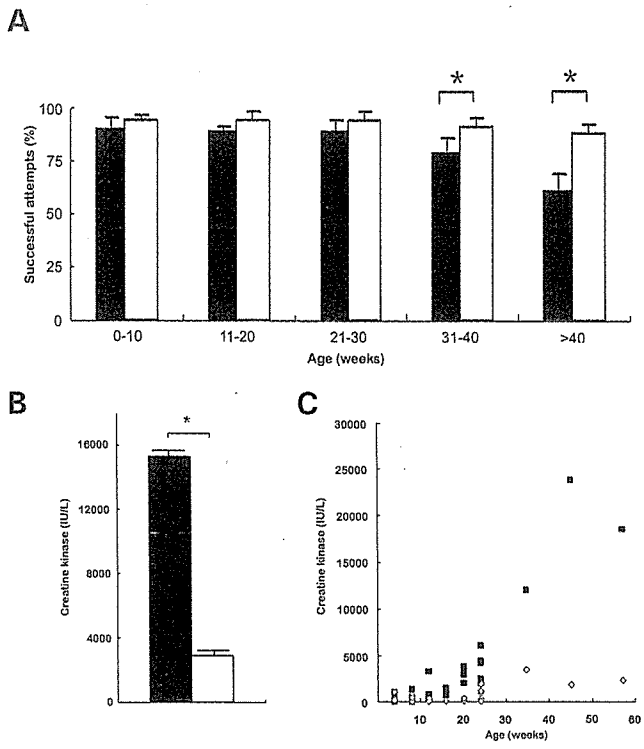

Figure 5. (**A**) Evaluation of over-all motor strength using rod-climbing test, according to age group. Mean of three trials are shown. $Gne^{(-/-)}$ h*GNE*V572L-Tg mice (closed bars, $n = 10$) perform worse than littermates ($n = 10$). Significant difference is noticeable after 30 weeks of age. Asterisk, $P < 0.05$ (Mann–Whitney U test). (**B**) Measurement of CK activity. Serum CK is significantly higher in $Gne^{(-/-)}$h*GNE*V572L-Tg mice (closed bars) when compared with littermates (open bars). Asterisk, $P < 0.05$ (Student's t-test, two-tailed). (**C**) CK activity according to age. CK activity of $Gne^{(-/-)}$ h*GNE*V572L-Tg mice (closed squares) starts to elevate after 30 weeks of age when compared with littermates (open diamonds).

Various proteins are expressed in the $Gne^{(-/-)}$h*GNE*V572L-Tg muscles

One of the defining hallmark features of DMRV/h-IBM is the presence of inclusion bodies that are presumed to have a role in muscle degeneration. These deposits have been shown to be immunoreactive to several proteins. Similar to human cases of DMRV, muscle cross sections obtained from the $Gne^{(-/-)}$ h*GNE*V572L-Tg mice reveal positive Congo red staining (Fig. 7D), which is not observed in the myofibers of control mice (data not shown). Intense, demarcated signals are seen within the area of RVs and more frequently co-localizing with inclusion bodies which are often seen in DMRV/h-IBM. As congophilia denotes deposition of proteins assuming a beta-pleated structure, we used the well-characterized 6E10, Aβ1–42, Aβ1–40 and A11 (amyloid β-oligomer), and β-site amyloid precursor protein cleaving enzyme (BACE2) antibodies to check for intracellular accumulation of amyloid. Amyloid depositions occur within the myofibers, and are seen to be occasionally associated with vacuolated fibers, as ~62% of RVs are positive for amyloid expression (data not shown). These amyloid inclusions are also noted in non-vacuolated fibers, including those which appear normal. Amyloid β precursor protein (AβPP), which is recognized by 6E10 antibody (Fig. 7I) has intense, large, fairly demarcated immunoreactive signals within the RVs, similar to the staining pattern of the fibrillar forms of amyloid β or amyloid β peptides 1–42 and 1–40 (Fig. 7J and K). In good agreement with finding amyloid deposits in the myofibers, BACE2, which purportedly represents β-secretase activity, is upregulated in these myofibers and are seen as granular staining in the cytoplasm and intense immunoreactivity at subsarcolemmal areas (Fig. 7H). Interestingly, the oligomer form of amyloid β, which is recognized by A11, is also expressed in the myofibers; positive signals are seen as aggregates around the RVs which are localized in areas distinct from fibrillar forms of amyloid (Fig. 7L).

We then analyzed skeletal muscles of mice from different age groups to see whether these amyloid accumulations are related to or can be considered as a function of age. We found out that these accumulations start to occur from 32 to 34 weeks of age, a period when virtually no RV is seen in the myofibers, and muscle pathology is characterized mainly by mild variation in fiber size (Fig. 8A and C). Both AβPP (Fig. 8B) and amyloid β 1–42 peptide (Fig. 8D) show positive immunoreactivity within the myofibers.

The microtubule-associated protein tau, a cytoskeletal protein, has been shown to be abnormally phosphorylated and accumulated in DMRV and other muscle disorders (21–23). Similarly, in these mice, these deposits are evident as squiggly inclusions which are occasionally seen in vacuolated fibers (Fig. 7M).

SM-31, an antibody which detects neurofilaments, has been well-characterized in DMRV/h-IBM (21,24). In muscle sections, positive staining is seen within the vicinity of RVs (Fig. 7N); not all RVs, however, show immunoreactivity with this antibody. SM-310, on the other hand, only stains the intramuscular nerve bundles (Fig. 7O).

Because of the accumulation of several proteins in the myofibers, ER stress and the unfolded protein response (UPR) have been implicated in the pathogenesis of DMRV/h-IBM. Using an antibody which recognizes one of the ER chaperones, we show that the UPR activation occurs in the $Gne^{(-/-)}$ h*GNE*V572L-Tg mice. Intracellular Grp-94 immunoreactivity is seen exclusively in vacuolated fibers (Fig. 7P). In the myofibers of the mice, strong reactivity to ubiquitin antibody in vacuolated and non-vacuolated fibers are seen (Fig. 7Q), suggesting that the ubiquitin–proteosome system may as well be involved in the degradation of abnormal protein accumulations in the muscle, and that misfolded proteins are ubiquitinated but not degraded.

Sarcolemmal proteins are also accumulated in DMRV/h-IBM myofibers. Within the vicinity of the RVs, positive α-dystroglycan (Fig. 7R), β-dystroglycan (Fig. 7S) and α-sarcoglycan (Fig. 7T) signals are observed.

In the myofibers of the control mice, no protein depositions were appreciated (data not shown).

Electron microscopic studies show evidence of autophagy and inclusions in the $Gne^{(-/-)}$h*GNE*V572L-Tg muscles

Ultrastructural studies confirm the activation of autophagy in $Gne^{(-/-)}$h*GNE*V572L-Tg muscles (Fig. 9). We obtained samples from a 42-week-old female mouse which had RVs

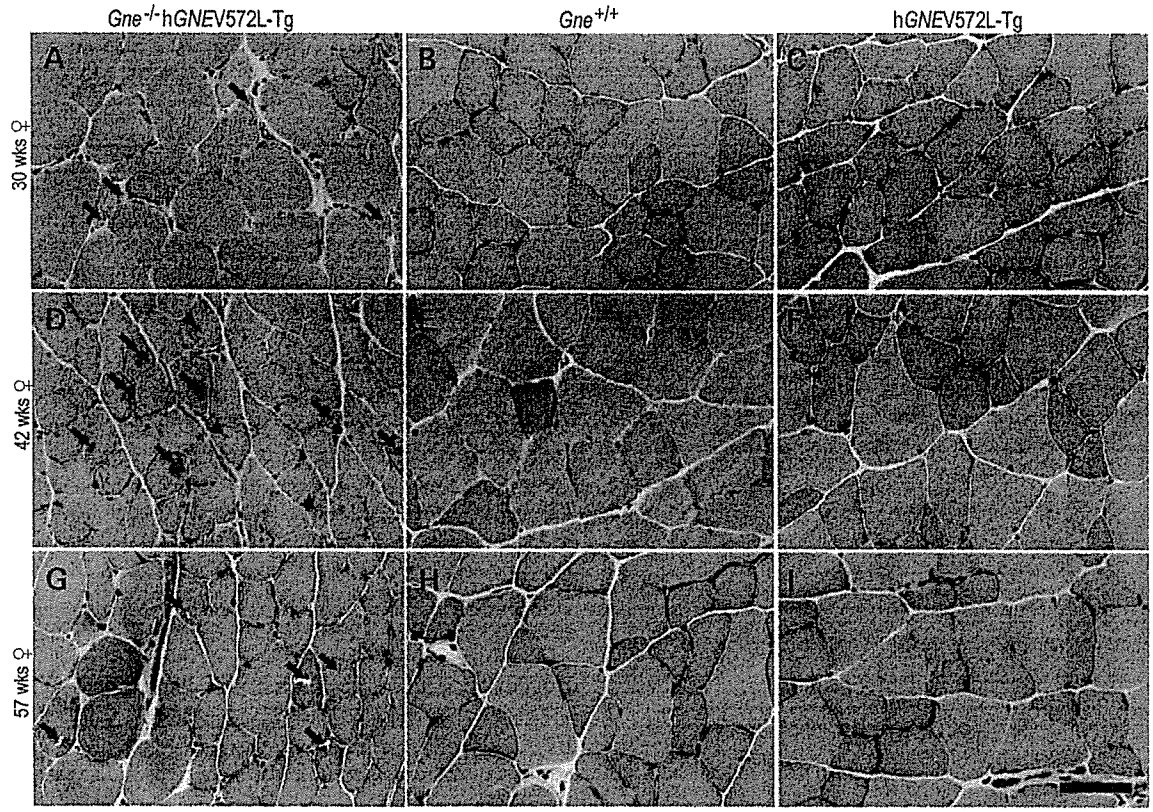

Figure 6. Hematoxylin and eosin sections from $Gne^{(-/-)}$h*GNE*V572L-Tg (**A, D, G**), WT (**B, E, H**), h*GNE*V572L-Tg (**C, F, I**). The h*GNE*V572L-Tg mice are comparable with WT in all ages. In the $Gne^{(-/-)}$h*GNE*V572L-Tg, there is variation in fiber size which becomes more obvious as the mice age. Fibrosis, necrotic or regenerating processes are not noted. Internalized nuclei are noted in scattered fibers. Small angular fibers are noted from around 30 weeks of age (A, arrows). Fibers with RVs (arrows), as well as cytoplasmic inclusions (arrowhead) are observed in scattered fibers from 42 weeks of age (D and G). Bar represents 40 μm.

as seen in light microscopy. In these samples, disorganization of myofibrils was seen in the vicinity of RVs. In about 500 myofibers examined, 10% showed ultrastructural evidence of autophagy. Collections of lysosomal autophagosomes containing undigested intracellular debris were seen, usually enclosed by a limiting membrane (Fig. 9A, arrow). The debris are often composed of light or electron-dense amorphous materials, and appeared like myelin whorls. Multiple small double membrane-bound autophagic vacuoles were often contained within a larger autophagic vesicle (AV), suggesting that autophagy in these myofibers involves a continual process of AV consolidation (Fig. 9A, arrowhead). Multilamellar bodies are also observed (Fig. 9A, double arrows). Probable amyloid deposits are seen as amorphous and granular material (Fig. 9B, magnified from A). Interestingly, ovoid and densely granular deposits, which may also be amyloid-like structures, are noted not only in the areas of autophagy (Fig. 9A, asterisk), but also in areas where myofibrillar architecture is well preserved (Fig. 9C). Occasionally, autophagic vacuoles are seen within the substance of these deposits (Fig. 9C, arrow).

$Gne^{(-/-)}$h*GNE*V572L-Tg shows pathological changes in the diaphragm and cardiac muscles

It has been a well-accepted fact that DMRV/h-IBM primarily involved the skeletal muscles, and that respiratory muscles are assumed to be spared as there had been no reports implying the involvement of the respiratory system. Interestingly, in the $Gne^{(-/-)}$h*GNE*V572L-Tg mice, we found that even diaphragm muscles are involved, although the findings range from almost normal findings to the presence of marked fibrosis and RVs in the myofibers (Fig. 10A). Likewise, we have observed inclusion bodies which are seen in both vacuolated and non-vacuolated fibers (data not shown).

It is now being recognized that some patients manifest with a variety of cardiac abnormalities, from the seemingly benign right bundle branch block to fatal arrhythmias. This led us to carefully check the status of cardiac muscles in the mice. We found out that few mice (around 20%) develop fibrosis in the cardiac tissue after the age of 30 weeks, and some show marked endomysial fibrosis (Fig. 10B). Moreover, amyloid deposition (Fig. 10C) and, occasionally, RVs (Fig. 10D) are also observed in cardiomyocytes. We also tried to functionally evaluate the heart using 2D echocardiography and electrocardiogram, but we did not observe any abnormality pointing to definite cardiomyopathy or conduction defects (data not shown), although we only tested a limited number of mice.

DISCUSSION

Sialylation of oligosaccharide chains is a common and physiologically important event, and sialic acids are probably the

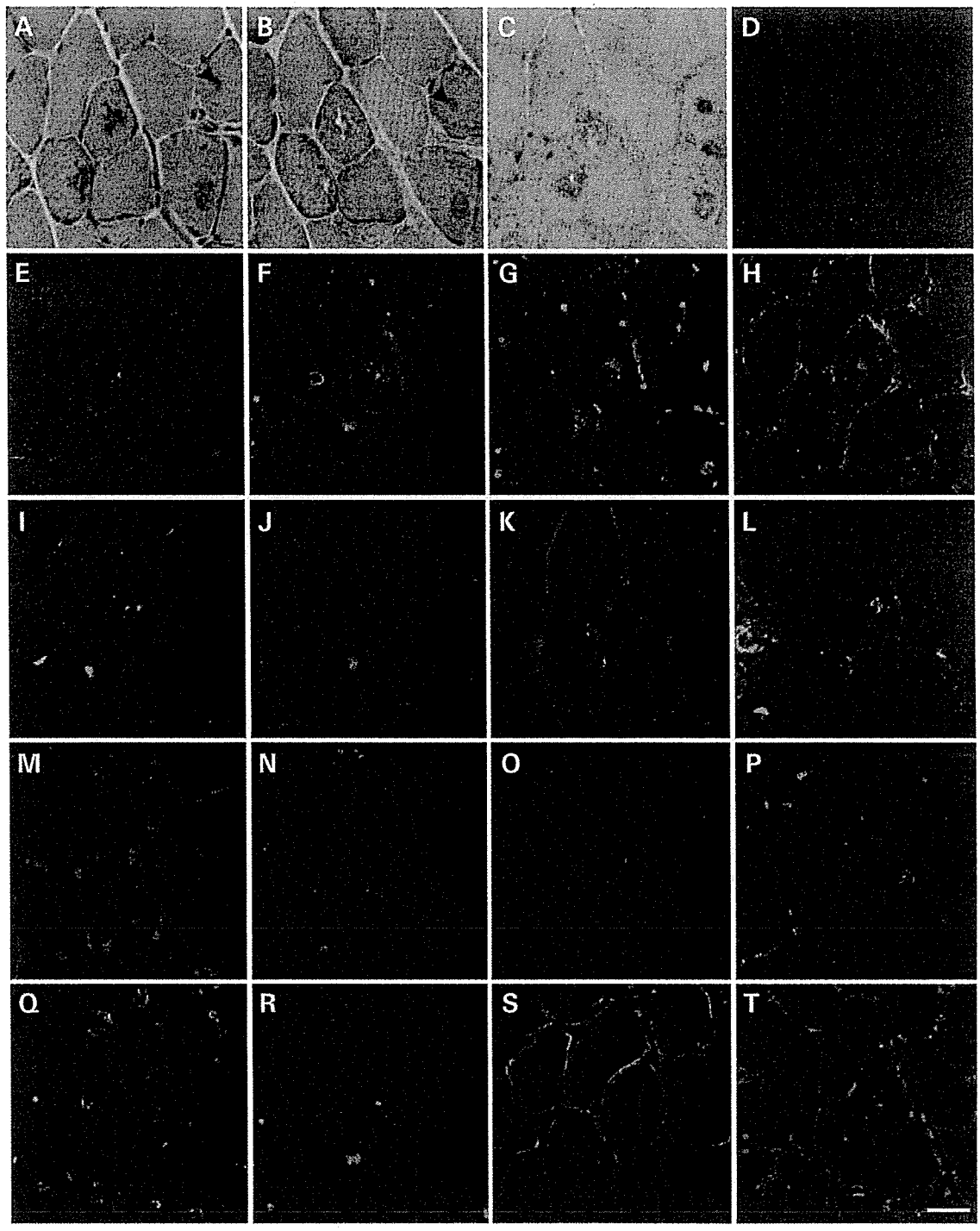

Figure 7. Serial sections taken from a 42-week-old female *Gne*$^{(-/-)}$h*GNE*V572L-Tg mouse. (**A**) Hematoxylin and eosin sections show fibers with RVs and cytoplasmic inclusions. (**B**) In modified Gomori trichrome, vacuoles are rimmed by eosinophilic granules. (**C**) Acid phosphatase activity is enhanced around RVs, suggesting upregulation of lysosomal activity in these areas. (**D**) Congo red staining visualized by Texas red filters shows positive staining in fibers with or without RVs, and appear as large, granular deposits. Immunoreactivity to lysosomal proteins confirm the presence of autophagy in fibers with RVs: (**E**) LAMP-1 signals are seen in the areas of RVs; (**F**) LAMP-2 has subsarcolemmal immunoreactivity, in addition to positive staining in RVs; (**G**) LC3 stains the same areas as LAMP-2, in addition to the perinuclear areas. Intracellular deposition of amyloid is seen in vacuolated or non-vacuolated fibers: (**H**) Increased reactivity to BACE2 is seen in the cytoplasm of fibers with RVs and within the vicinity of RVs; (**I**) AβPP expression is intense in area of RVs, seen as discrete deposits; (**J**) amyloid β 1–42 and (**K**) amyloid β 1–40 stainings are likewise seen as discrete deposits within the vicinity of RVs; (**L**) amyloid β-oligomeric antibody signals are noted as aggregates of small granule-like deposits around the RVs. Neurofilament deposition is observed in the myofibers: SM-31 (**M**) immunoreactivity is occasionally noted within the vicinity of RVs, whereas SM-310 (**N**) only stains intramuscular nerve bundles. (**O**) Epitopes of phosphorylated tau are observed in some fibers with RVs. (**P**) Fibers with RVs have intense ubiquitin staining around RVs and granule-like signals in these fibers. (**Q**) Grp94, an endoplastic reticulum luminal stress protein, is upregulated exclusively in vacuolated fibers as large granular deposits within the RVs. Sarcolemmal proteins are deposited within the vicinity of RVs: (**R**) α-dystroglycan; (**S**) β-dystroglycan; and (**T**) α-sarcoglycan. Bar represents 20 μm.

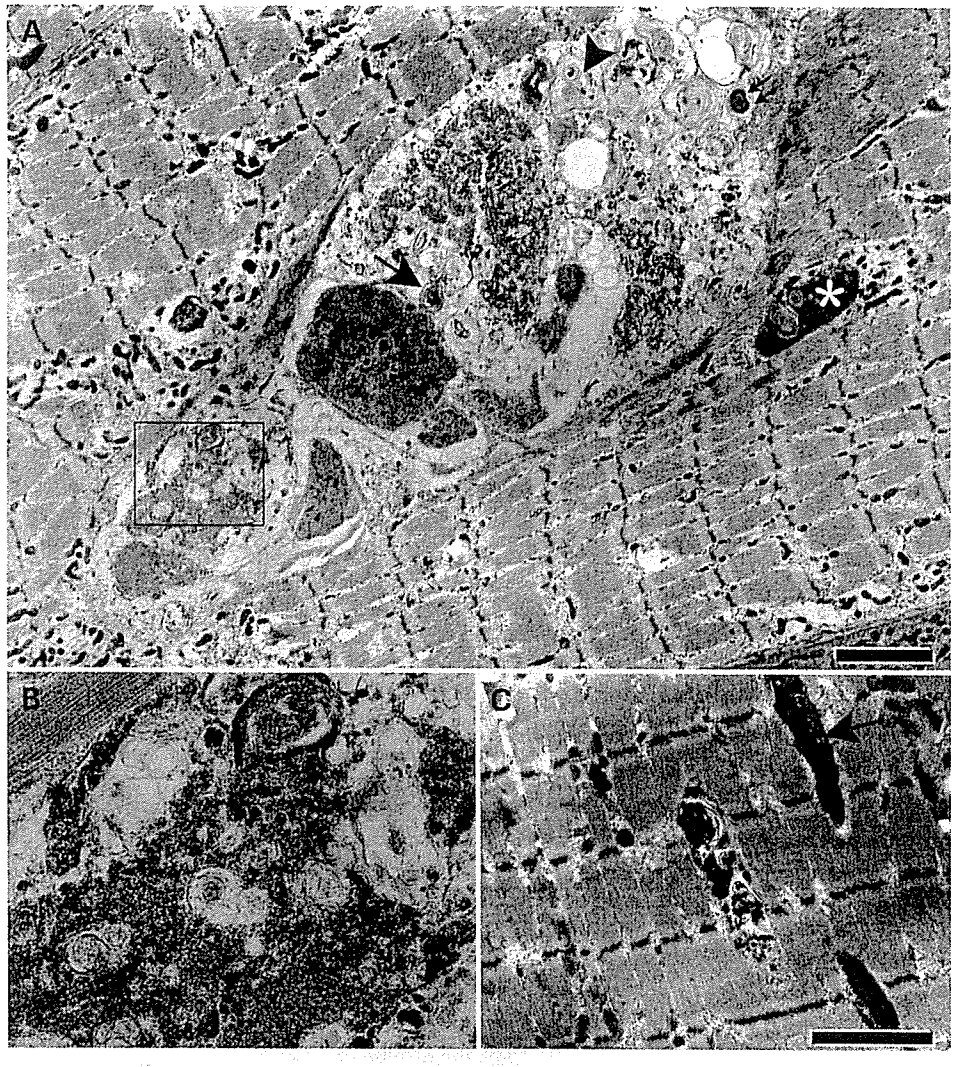

Figure 8. Ultrastructural evidence of autophagy and intracellular inclusions. (**A**) Collections of lysosomal autophagosomes with intracellular debris which are light or electron-dense amorphous materials enclosed by a limiting membrane (arrow). Multilammelar structures are also observed (double arrows). Ovoid and dense deposits which are probably amyloid deposits are likewise seen (asterisk) (**B**) Probable amyloid deposits are seen as amorphous and granular material surrounded by autophagosomes (B, magnified from A). (**C**) Dense, granular deposits which are probably amyloid accumulations are also noted in areas where architecture of myofibrils are generally well preserved; occasionally, autophagic vacuoles are seen within the substance of these deposits (arrow). Bar represents 2 μm.

most biologically important monosaccharide units of glycoconjugates. These negatively charged sugars at the terminal ends of glycoconjugates have very important biological roles in mammalian development, and this is underscored by the embryonic lethality resulting from attempts to knock-out *Gne* in the mice (20), and further supported by the absence of homozygous null mutations in humans. Making a transgenic *GNE* mouse on a *Gne* knockout background thus allowed us to rescue the phenotype in *Gne* knockout. Clearly, the $Gne^{(-/-)}$h*GNE*V572L-Tg resembles the phenotype in human DMRV/h-IBM patients.

It is conceivable that a mutation in the *GNE*, a gene responsible for catalyzing the rate-limiting step in sialic acid biosynthesis, can lead to hyposialylation. Most, if not all, of the mutations causing DMRV caused partial reduction of the enzymatic activity of either UDP-GlcNAc 2-epimerase or ManNAc kinase of the GNE (17,19). As we have predicted, our results show that there is a marked reduction in sialic acid level, which can reflect the enzymatic activity of GNE, in the serum and other tissues of the $Gne^{(-/-)}$h*GNE*V572L-Tg mice. With regards to the expression of *GNE* in various tissues, it has been shown that expression in the muscle is very low (25). Our results show, on the other hand, that mRNA expression of h*GNE*V572L-Tg is highest in the muscle, and we attribute this to the promoter that we used in the transgene construct. Previously, we have shown that CAG promoter efficiently promotes expression of a gene into adult skeletal muscles (26).

Skeletal muscle is mainly affected in DMRV/h-IBM, although it is reasonable to expect multi-organ involvement because of the ubiquitous expression of *GNE*. In our mice, the skeletal muscle is clearly affected despite the data that